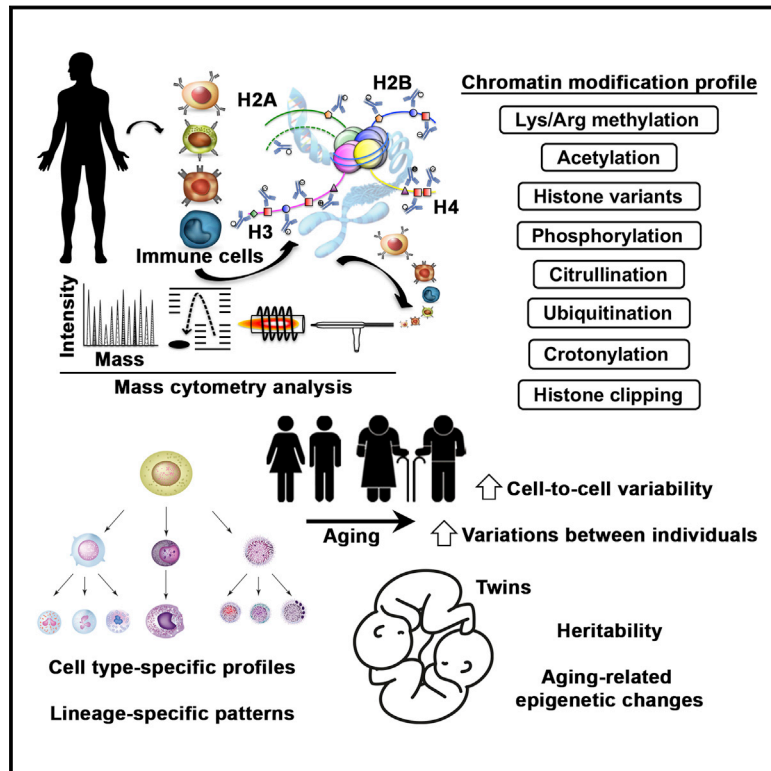


Single-Cell Chromatin Modification Profiling Reveals Increased Epigenetic Variations with Aging

Graphical Abstract



Authors

Peggie Cheung, Francesco Vallania, Hayley C. Warsinske, ..., Paul J. Utz, Purvesh Khatri, Alex J. Kuo

Correspondence

pjutz@stanford.edu (P.J.U.),
pkhatri@stanford.edu (P.K.),
alex0229@stanford.edu (A.J.K.)

In Brief

A global look at human chromatin shows that variability in histone modification patterns accrues with age and depends on non-heritable factors.

Highlights

- Diverse chromatin marks in single cells are measured by mass cytometry
- Cell-type-specific profiles of chromatin marks predict immune cell identity
- Chromatin variations between individuals and single cells increase with age
- Aging-related alterations of chromatin are largely driven by non-heritable factors

Single-Cell Chromatin Modification Profiling Reveals Increased Epigenetic Variations with Aging

Peggie Cheung,^{1,2,7} Francesco Vallania,^{1,3,7} Hayley C. Warsinske,^{1,3} Michele Donato,^{1,3} Steven Schaffert,^{1,3} Sarah E. Chang,^{1,2} Mai Dvorak,^{1,2} Cornelia L. Dekker,⁴ Mark M. Davis,^{1,5,6} Paul J. Utz,^{1,2,*} Purvesh Khatri,^{1,3,*} and Alex J. Kuo^{1,2,8,*}

¹Institute for Immunity, Transplantation, and Infection, Stanford University School of Medicine, Stanford, CA 94305, USA

²Department of Medicine, Division of Immunology and Rheumatology, Stanford University School of Medicine, Stanford, CA 94305, USA

³Department of Medicine, Division of Biomedical Informatics Research, Stanford University School of Medicine, Stanford, CA 94305, USA

⁴Department of Pediatrics, Stanford University School of Medicine, Stanford, CA 94305, USA

⁵Department of Microbiology and Immunology, Stanford University School of Medicine, Stanford, CA 94304, USA

⁶Howard Hughes Medical Institute, Stanford University School of Medicine, Stanford, CA 94304, USA

⁷These authors contributed equally

⁸Lead Contact

*Correspondence: pjutz@stanford.edu (P.J.U.), pkhatri@stanford.edu (P.K.), alex0229@stanford.edu (A.J.K.)

<https://doi.org/10.1016/j.cell.2018.03.079>

SUMMARY

Post-translational modifications of histone proteins and exchanges of histone variants of chromatin are central to the regulation of nearly all DNA-templated biological processes. However, the degree and variability of chromatin modifications in specific human immune cells remain largely unknown. Here, we employ a highly multiplexed mass cytometry analysis to profile the global levels of a broad array of chromatin modifications in primary human immune cells at the single-cell level. Our data reveal markedly different cell-type- and hematopoietic-lineage-specific chromatin modification patterns. Differential analysis between younger and older adults shows that aging is associated with increased heterogeneity between individuals and elevated cell-to-cell variability in chromatin modifications. Analysis of a twin cohort unveils heritability of chromatin modifications and demonstrates that aging-related chromatin alterations are predominantly driven by non-heritable influences. Together, we present a powerful platform for chromatin and immunology research. Our discoveries highlight the profound impacts of aging on chromatin modifications.

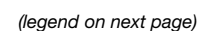
INTRODUCTION

Histone proteins are subject to a wide range of covalent post-translational modifications (PTMs), such as phosphorylation, acetylation, and methylation. These chemical moieties alter the architecture of chromatin (Kouzarides, 2007) or serve as docking sites for “reader” proteins that dictate higher-order chromatin compaction or recruit protein complexes with DNA-related biological functions (Taverna et al., 2007). Cell-cycle-independent incorporation of histone variants further diversifies chromatin

states and provides an additional layer of regulation to DNA-templated processes (Maze et al., 2014). Nucleosomes constituted with histone variants change the structure and stability of chromatin and, through unique protein motifs or variant-specific PTMs, alter interactions with chromatin binding proteins (Talbert and Henikoff, 2017). Collectively, chromatin modifications (chromatin marks), including histone PTMs and histone variants, along with the underlying DNA, regulate epigenetic phenotypes.

Despite the crucial roles of chromatin marks in diverse physiological functions and human diseases, studying chromatin biology in human immune cells has been challenging. While recent technologic breakthroughs have allowed investigations of chromatin dynamics using a small number of cells or even single cells (Buenrostro et al., 2015; Corces et al., 2016; Gomez et al., 2013; Rotem et al., 2015; Schwartzman and Tanay, 2015), a high-throughput method to measure the overall cellular levels of chromatin marks in individual cells has not been described.

Here, we report the development of epigenetic landscape profiling using cytometry by time-of-flight (EpiTOF) to measure the cellular levels of 8 classes of histone modifications and 4 histone variants, in 22 major immune cell subsets. The high-dimensional and single-cell nature of these datasets allow the creation of an immune cell epigenetic atlas based on their chromatin modification profiles. EpiTOF analysis of 24 healthy cytomegalovirus (CMV)-seronegative subjects reveals cell-type-specific chromatin modification profiles in quiescent immune cells and distinct patterns shared by cells derived from lymphoid and myeloid lineages. Unique profiles of chromatin marks in single cells form a molecular signature that can predict immune cell identity. Further, EpiTOF identifies differential chromatin marks between CD56^{bright} and CD56^{dim} natural killer (NK) cells, between naive and memory T cell subsets, and in regulatory T cells. Recent reports have found substantial chromatin changes as a result of aging (Moskowitz et al., 2017; Ucar et al., 2017). Comparative analysis of younger and older adults reveals that increased variations between individuals and elevated cell-to-cell variability in chromatin marks are signatures of aging. Through analysis of 19 twin pairs, we find that 70% of



the chromatin modification variance is explained by environmental influences. Divergent chromatin modification profiles in older monozygotic twin pairs than in younger pairs indicate that increased variations of chromatin marks with age are largely attributed to non-heritable factors. Together, we develop a high-throughput multiplexed assay to interrogate chromatin modifications at the single cell level in the human immune system. Our data provide insights about how aging affects the epigenomic landscape and the relative contribution of nature and nurture to chromatin dynamics in aging human cells.

RESULTS

Establishment of EpiTOF for Profiling Chromatin Marks in Single Cells

We leveraged the highly multiplexed capacity and single-cell resolution of mass cytometry (Bendall et al., 2011) to develop EpiTOF for simultaneous measurement of chromatin marks in single immune cells. We characterized over 150 commercial antibodies to create panels of highly specific antibodies directed against chromatin marks. Strategies used to validate individual antibodies included ectopic overexpression or RNAi- or CRISPR-mediated depletion of chromatin modifying enzymes, cell stimulations, and treatments with small molecules such as the lysine methyltransferase EZH2 inhibitor, Tazemetostat (Data S1). We selected 40 validated antibodies to construct two panels of lanthanide-labeled antibodies for EpiTOF (Table S1). Two antibodies targeting total histone proteins, one against the globular domain of H3 and one against the unstructured tail of H4, were integrated to control for variations in histone expression, nuclear epitope accessibility and antibody background. Together with immunophenotypic markers to reveal the identity of immune cells and channels for viability and sample barcodes, over 70 parameters were analyzed in each sample (Figure 1A).

Cell-Type-Specific Chromatin Modification Profiles in Healthy Immune System

We analyzed peripheral blood mononuclear cells (PBMCs) purified from 12 healthy CMV-seronegative subjects, comprising

6 subjects under 25 years old (3 males; 3 females) and 6 subjects over 65 years old (3 males; 3 females) (bio rep 1) and replicated our results in an independent 12-subject cohort with identical demographics (bio rep 2) (Figure 1B). A linear regression model was applied to perform data normalization for each chromatin modification using total histones as predictor variables. After normalization, we found that CD14⁺ monocytes contain abundant proteolytically cleaved histone H3 at threonine 22 (cleaved H3 Thr22) and express higher levels of peptidylarginine deiminase 4 (PADI4) relative to B, T, and NK cells (Figures 1C and S1A). In contrast, monocytes contain reduced levels of the histone variant H3.3 and tri-methylation of histone H3 at lysine 27 (H3K27me3). Within the lymphocyte compartment, CD4⁺ and CD8⁺ T cells share similar patterns, whereas NK cells contain reduced levels of a broad range of chromatin marks than other cell subtypes. Chromatin marks known to be present at low levels in unperturbed cells, such as DNA double-strand break-induced γ -H2AX (Rogakou et al., 1998), and citrullination marks (Cuthbert et al., 2004; Wang et al., 2004b) had very low signals in EpiTOF. Despite distinct genetic backgrounds between the 12 subjects, Inverse Simpson's Diversity Index (ISDI) analysis showed modest subject-to-subject variability in chromatin marks, with acetylation of H3 at lysine 14 (H3K14ac), cleaved H3 Thr22 and H2A.Z showing the most variability (average ISDI = 36%, 45%, and 47%, respectively) and macroH2A, PADI4, and ubiquitination of H2B at lysine 120 (H2BK120ub) demonstrating the least variability (average ISDI = 85%, 82%, and 79%, respectively) between subjects. Together, our results indicate that individual immune cell subtypes are characterized by distinct profiles of chromatin marks.

Next, monocytes, B, T, and NK cells were sorted by fluorescence-activated cell sorting (FACS) independently from two subjects for western blot analysis (Figures 1D and S1B). The results agreed with the normalized mark levels by EpiTOF across several classes of chromatin modifications. EpiTOF analysis on 6 subjects in duplicate showed a correlation coefficient of 0.96 between replicates, demonstrating high technical reproducibility (Figure S1C). Further, between the two biological replicates, the correlation coefficient of 0.93 (Figure S1D) suggests that the

Figure 1. Lineage-Specific Chromatin Modification Profiles in Human Immune Cells

- (A) Overview of the EpiTOF platform.
 (B) Experimental design. Two EpiTOF panels measuring 9 classes of chromatin marks were employed to analyze PBMCs derived from a cohort containing 12 healthy CMV-seronegative subjects (bio rep 1) and an independent cohort with identical demographics (bio rep 2).
 (C) Cell-type-specific chromatin modification profiles in major immune cell subsets. EpiTOF analysis of subjects from bio rep 1. Heatmap representation of the normalized chromatin mark levels of the indicated 40 chromatin marks (x axis) in 11 major immune cell subsets (y axis). The normalized mark levels are centered on the mean of the total PBMCs. Minimum and maximum values are shown. Color, mean across 12 subjects; dendrograms, unsupervised clustering at both axes; and diameter of circle, subject-to-subject variability measured by Inverse Simpson's Diversity Index.
 (D) Validation of EpiTOF data by western blotting on sorted immune cells. Western blot analysis of the whole-cell extract from sorted immune cells using the indicated antibodies.
 (E) Higher expression of lysine methyltransferases *EZH1* and *EZH2* in common lymphoid progenitors (CLP) than in common myeloid progenitors (CMPs). Gene expression analysis of *EZH1* and *EZH2* in CLPs (blue) and CMPs (red) using a publicly available RNA-seq dataset: GEO: GSE74246. y axis, expression levels of the indicated genes.
 (F) Differential enrichment of H3K27me3 and H3K4me3 are associated with gene expression reprogramming during lymphoid and myeloid lineage commitment. Top: Venn diagrams show the numbers of overlapping genes between genes enriched with H3K27me3 (left light-blue circle) or H3K4me3 (right light-blue circle) in T cells over monocytes and differentially expressed genes in CLPs over CMPs (left pink circle, lower expression in CLPs over CMPs; right pink circle, higher expression in CLPs over CMPs). Numbers of shared genes and p values of the overlaps are shown. Bottom: gene ontology enrichment analysis using the overlapped genes from the two Venn diagrams. p values for enrichment with the indicated gene ontology terms and examples of shared genes in each Venn diagram are shown.

See also Figure S1, Table S1, and Data S1.

heatmaps in [Figures 1C](#) and [S1A](#) represent the chromatin modification profiles in healthy human immune system.

Lineage-Specific Chromatin Modification Profiles

Unsupervised clustering of immune cells by chromatin modification profiles revealed that cells from lymphoid and myeloid lineages contain distinct patterns of chromatin marks (y axis in [Figures 1C](#) and [S1E](#)). Reduced H3.3 and H3K27me3 and elevated cleaved histone H3 Thr22, mono-methylation of H3 at lysine 36 (H3K36me1), and the expression of *PADI4* are signatures of myeloid cells relative to lymphocytes. The profile of chromatin marks in Lin[−]CD45^{dim}CD34⁺ hematopoietic progenitors resembles the patterns in myeloid cells. Using publicly available RNA sequencing (RNA-seq) data from sorted immune cells (GEO: GSE74246) ([Corces et al., 2016](#)), we found that the expression of *EZH1* and *EZH2*, the two lysine methyltransferases catalyzing H3K27me3, is significantly higher in common lymphoid progenitors (CLPs) and in peripheral T cells than in common myeloid progenitors (CMPs) and in monocytes ([Figures 1E](#) and [S1F](#)). The results support a model in which divergence of H3K27me3 occurs during CLP and CMP differentiation, and the profiles are established during the commitment of hematopoietic stem cell to common lymphoid or myeloid progenitors. Together, we conclude that the cell-type-specific chromatin modification profile is indicative of the hematopoietic lineages from which individual populations are derived.

To investigate the influences of altered chromatin modifications on gene expression programming during hematopoiesis, we performed analysis on a chromatin immunoprecipitation sequencing (ChIP-seq) dataset (GEO: GSE18927) from the Roadmap Epigenomics Mapping Consortium, where hallmarks of gene silencing and active transcription and H3K27me3 and H3 tri-methylation at lysine 4 (H3K4me3), respectively, were profiled in sorted peripheral CD3⁺ T cells and CD14⁺ monocytes ([Bernstein et al., 2010](#)). In agreement with EpiTOF findings, H3K27me3 showed higher peak intensity in T cells, whereas the peak intensity of H3K4me3 was higher in monocytes ([Figure S1G](#)). Similarly, using a false discovery rate (FDR) of 5% as threshold we identified more genes differentially enriched with H3K27me3 in T cells than in monocytes (7,048 vs. 4,008) but fewer genes differentially enriched with H3K4me3 in T cells than in monocytes (637 vs. 4,097). Comparison with a transcription profiling dataset (GEO: GSE74246) ([Corces et al., 2016](#)) revealed that H3K27me3-enriched genes were transcriptionally repressed and H3K4me3-enriched genes were actively transcribed, indicating comparable transcription activities and chromatin modification profiles between both datasets. Among 7,048 genes enriched with H3K27me3 in T cells, a significant proportion ($n = 1,590$, $p < 2.2 \times 10^{-16}$) was transcriptionally repressed in CLPs in comparison with the expression in CMPs (FDR < 5%) ([Figure 1F](#)). The results suggest that this group of genes is differentially regulated, at the levels of both H3K27me3 enrichment and transcription, during the lineage commitment of CLPs and CMPs. Gene ontology (GO) enrichment analysis revealed that a significant number of these genes are involved in the differentiation of megakaryocyte-erythroid progenitors (MEPs) and granulocyte-monocyte progenitors (GMPs), such as *GATA1*, *PU.1*, and *C/EBP α* ([Pevny et al., 1991](#); [Scott et al.,](#)

[1994](#); [Zhang et al., 1997](#)), in addition to myeloid cell-specific markers, such as *CD33* and *PADI4*. Similarly, 97 of 637 genes ($p < 3.8 \times 10^{-11}$) enriched with H3K4me3 in T cells are upregulated in CLPs relative to CMPs (FDR < 5%), whose programming of H3K4me3 and transcription also likely occurs during CLP and CMP lineage commitment. This group of genes contains key regulators of lymphocyte differentiation, such as *BLIMP1*, *FOXP1*, and *IL7R* ([Hu et al., 2006](#); [Mazzucchelli and Durum, 2007](#); [Turner et al., 1994](#)). Together, the results support a model in which chromatin modification profiles undergo drastic changes and are associated with gene expression reprogramming during hematopoietic lineage determination, in accordance with our EpiTOF findings.

Chromatin Modification Profiles Predict Immune Cell Identity

Principal component analysis (PCA) using single-cell EpiTOF data distinguished between immune cell types based on the profiles of chromatin marks ([Figures 2A](#) and [S2A](#)), suggesting that cells within the same subset share a cell-type-specific pattern. Euclidean distances computed from chromatin modification profiles between immune cell subtypes found the greatest separation between monocytes and various lymphocyte subsets, reflecting the divergence between lymphoid and myeloid lineages. Distances between lymphocyte subtypes are approximately 4-fold lower than those between monocytes and lymphocytes ([Figures 2A](#) and [S2A](#)).

Next, we used L-1 regularized logistic regression models ([Friedman et al., 2010](#)) to classify immune cells based on chromatin marks alone utilizing single-cell data from bio rep 1 as the training dataset. Using either EpiTOF panel, monocytes, B, T, and NK cells can be distinguished from the remaining PBMCs with high accuracy ([Figure 2B](#)). We validated the models with the single-cell data from bio rep 2. The coefficients derived from bio rep 1 ([Table S2](#)) accurately identified the corresponding immune cell types in bio rep 2 ([Figure 2C](#)). These results demonstrate that a set of chromatin marks form an epigenetic signature that allows accurate prediction of immune cell identity.

Differential Chromatin Marks in T Cell Functional Subsets

Next, we developed T-cell-focused EpiTOF panels measuring the levels of 40 chromatin marks in 11 T cell subsets ([Table S3](#)) to analyze the same cohorts described above ([Figures 3A](#) and [S3A](#)). A correlation between the two biological replicates demonstrates high biological reproducibility of our results ([Figure S3B](#)). Unsupervised clustering based on chromatin marks revealed that T cells expressing $\alpha\beta$ T cell receptors (TCRs) are characterized by a distinct chromatin modification profile when compared with T cells expressing $\gamma\delta$ TCRs, which have specialized functions in immune responses ([Chien et al., 2014](#)) ([Figures 3A](#) and [S3A](#)). Both CD4⁺ and CD8⁺ CD197⁺CD45RO[−] naive T cells clustered together. In contrast, CD197[−]CD45RO[−] effector and CD45RO⁺ memory subsets showed divergence in chromatin marks from the naive populations. The results demonstrate the plasticity of chromatin marks in T cells, which are likely reconfigured as they differentiate to assume specialized immunological functions in adaptive immunity.

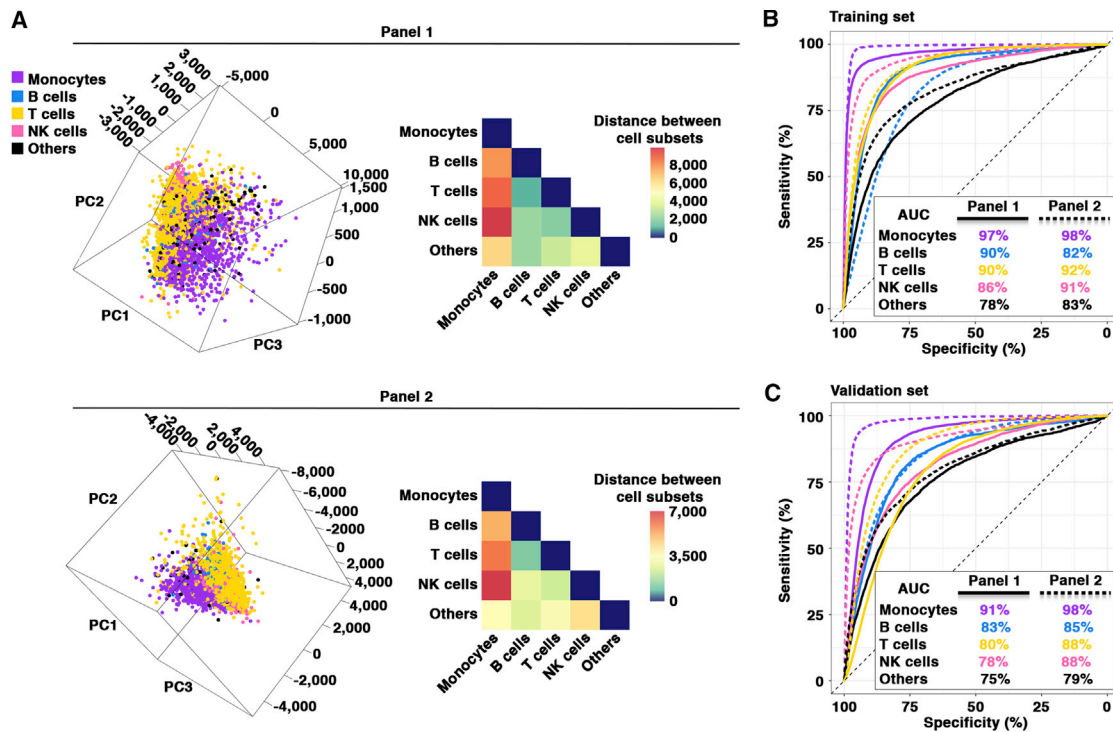


Figure 2. Single-Cell Chromatin Modification Profile Predicts Immune Cell Identity and Uncovers Relationships between Chromatin Marks

(A) Segregation of immune cell subsets based on chromatin modification profiles. Left: PCA of single-cell EpiTOF data described in Figure 1C (bio rep 1). Each dot represents a single cell, and each principal component depicts variations of 20 chromatin marks measured using each EpiTOF panel. Analyses using single-cell data collected by EpiTOF panel 1 (top) and 2 (bottom) are shown. Cells are color-coded by immune cell types. Right: Euclidean distances of chromatin modification profiles between the indicated immune cell subtypes.

(B and C) Patterns of chromatin modifications in single-cells predict immune cell identity. ROC curves discriminate between the indicated immune cell lineages from the remaining PBMC subsets using a regularized logistic regression model. The AUCs, which measure the sensitivity and specificity of the separation for the indicated cell types, are shown (B). The model from (B) (training dataset, bio rep 1) is applied to the validation dataset (bio rep 2) to test prediction power. ROC curves and AUCs from the validation dataset are shown (C).

See also Figure S1 and Table S2.

Differentiation of naive to memory cells is associated with marked changes in the chromatin modification profile (Figure 3B). Consistent trends were found in CD4⁺ and CD8⁺ T cells in both biological replicates. In memory T cells, phosphorylation of H3 at serine 10 (H3S10ph), which is detected at the transcription start sites of actively transcribed genes (Agalioti et al., 2002), is highly elevated. Together with the discoveries of higher euchromatin-associated H3K27me1 and H3K36me1 (Barski et al., 2007; Wagner and Carpenter, 2012) and lower heterochromatin-associated H3K27me3, H4K20me3, and H3K9me2 (Trojer and Reinberg, 2007) in memory T cells, our results suggest that chromatin in memory T cells is maintained in a more accessible state than in the naive subsets.

Differential analysis of chromatin marks in CD4⁺CD25⁺FOXP3⁺ regulatory T cells (Tregs) over total CD4⁺ T cells revealed that H3K27me1 and H3K27ac are highly elevated in Tregs, in addition to a reduction in H3K27me3 (Figure 3C). The essential roles of EZH2 in the functions of Tregs have been studied extensively (Arvey et al., 2014; DuPage et al., 2015). We found that in addition to the upregulation of EZH1 and EZH2 in Tregs, the expression of KDM6A/UTX and KDM6B/JMJD3, which catalyze H3K27 demethylation (Shi, 2007), is also elevated

(Figure S3C). Our data highlight the importance of studying the biological significance of lower H3K27 methylation state and H3K27ac in Tregs (Li et al., 2014).

Profiles of Chromatin Marks Segregate CD56^{bright} NK Cells from the CD56^{dim} Subset

In CD56⁺ NK cells, chromatin marks measured by EpiTOF panel 1 showed especially high coefficient of variation (CV) (data not shown). We thus performed PCA to examine the relationships between the variations of the 20 chromatin marks in EpiTOF panel 1 and the two classical NK cell markers, CD56 and CD16 (Figures 3D and S3D). PC1 explained 80.1% of the variance and separated NK cells into two subsets. The bimodal distribution of PC1 score was highly similar to the segregation by MixTools using CD56 (Benaglia et al., 2009). The CD56^{dim} subset, which accounts for approximately 90% of total NK cells, has stronger cytotoxic killer cell functions than the low-abundance CD56^{bright} population (Lanier et al., 1986), whereas the latter is the major source of secreted cytokines (Cooper et al., 2001). EpiTOF analysis identified several increased acetylation marks in the CD56^{bright} subset. PADI4 expression and cleaved histone H3 Thr22, the two myeloid

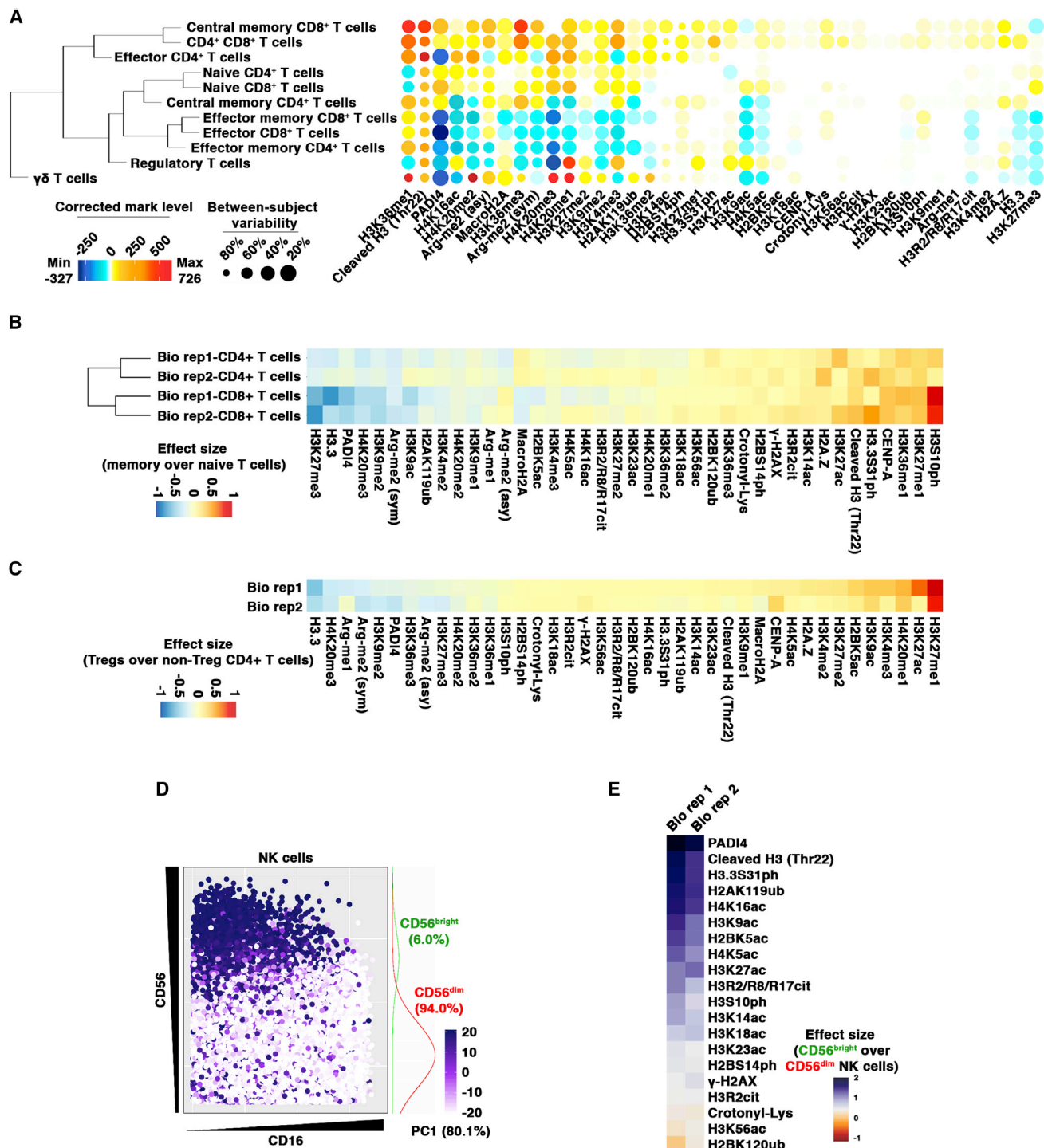


Figure 3. Heterogeneity of Chromatin Modification Profiles in Lymphocytes Originated from Diverse Functional Subsets

(A) T-cell-specific chromatin modification profiles. EpiTOF analysis on the same cohort used in Figure 1C (bio rep 1) focusing on T cell subsets. Heatmap representation of the normalized chromatin mark levels used in Figure 1C for the indicated 40 chromatin marks (x axis) in 11 T cell subsets (y axis). The normalized mark levels are centered on the mean of total CD3⁺ T cells. Minimum and maximum values of normalized mark levels are shown. The mean of each chromatin mark and T cell subset pair across 12 subjects is used for plotting. Dendrograms, unsupervised clustering; diameter of circle, subject-to-subject variability measured by Inverse Simpson's Diversity Index.

(B) Memory T cells are characterized by unique patterns of chromatin marks. Heatmap representation of the effect sizes of the levels of 40 chromatin marks in the indicated memory T cells over the naive subsets in both biological replicates. Dendrogram at y axis, unsupervised clustering.

(legend continued on next page)

lineage-specific markers, were higher in the CD56^{bright} subset (Figure 3E). Reanalyzing PBMC EpiTOF data revealed that the CD56^{bright} NK cells do not cluster with the CD56^{dim} population or with other lymphocytes (Figure S3E). While the CD56^{bright} subset is historically considered the precursor of CD56^{dim} NK cells, recent evidence suggests that the two subsets differentiate from independent hematopoietic lineages (Wu et al., 2014). Our data provide insights into the ontological relationships at the level of chromatin between both NK cell subsets.

EpiTOF Reveals Aging-Associated Changes in Chromatin Modification Profiles and Increased Heterogeneity between Individuals

Hallmarks of aging include declining hematopoietic output, defective immune cell functions, and an elevated proportion of CD45RO⁺ memory T cell subsets as we observed in our cohort (Figure S4A) (Wertheimer et al., 2014). Next, we compared chromatin modifications in younger (<25 years) and older (>65 years) subjects from both biological replicates. To increase statistical power, data from both biological replicates were merged for combined analysis (Figure S4B). CD4⁺ and CD8⁺ T cells in the original EpiTOF analysis (Figures 1C and S1A) were replaced with the data from the T-cell-focused analyses (Figures 3A and S3A), creating an atlas of 40 chromatin marks in 20 immune cell types (800 data points) for each of the 24 healthy participants (Figure 4A). PCA of 800 data points revealed that PC 1 and 2, which together explained 72.7% of the variance in the dataset, best separated the subjects by age, whereas sex had negligible contribution to the variance (Figure 4B). Notably, the chromatin modification profiles in younger subjects were relatively homogeneous; in contrast, heterogeneity markedly increased among older subjects. The levels of the vast majority of the 800 data points were elevated in older subjects in both biological replicates (Figures 4C and S4C). This was not due to changes in total histone content, as the cellular levels of histone H3 and H4 were not significantly different between younger and older subjects (Figure S4D). Collectively, we found that with age the levels of a wide range of chromatin marks increase in diverse immune cell types.

In contrast, 34 of the 40 chromatin marks in CD45RO⁺CD197⁺ central memory CD8⁺ T cells were repressed in older subjects (Figure 4C). This observation is accompanied by statistically significant reductions in both histone H3 and H4 (Figure S4D). Aging-associated histone loss has been reported in several species, and reduced nucleosome occupancy with age has been implicated in changes in chromatin dynamics and transcription activities (Booth and Brunet, 2016). Our results suggest a unique mode of aging at chromatin in central memory CD8⁺ T cells.

Increased Cell-to-Cell Variability in Chromatin Modifications with Age

Recent publications have described increased variability in the immune systems of older versus younger human beings (Brodin and Davis, 2017; Kaczorowski et al., 2017). To test if cell-to-cell variability in chromatin modifications changes with age, we performed multiple t tests comparing CVs of 40 chromatin marks in 20 immune cell subsets at the single-cell level between younger and older subjects. Strikingly, we found that 61.8% of the 800 tests showed increased single-cell variability in older subjects (Figure S5A). After correcting for multiple hypotheses, out of 30 significant chromatin mark and cell-type pairs (FDR < 5%), 29 tests showed higher cell-to-cell variability in older subjects (Figure 5A). We conclude that increased cell-to-cell variability in chromatin marks is a signature of aging in immune cells.

Elevated Single-Cell Variability in Polycomb-Repressive Complex-Mediated Modifications with Age

Among the 29 chromatin mark- and cell-type combinations that showed a statistically significant increase in CV in older subjects (FDR < 5%), more than 50% (17 of 29) involved H3K27me3, H3K27me2, and H2AK119ub, all of which are catalyzed by polycomb-repressive complex 1 or 2 (PRC1 or PRC2) (Di Croce and Helin, 2013; Wang et al., 2004a) (Figure 5B). Increased cell-to-cell variability with age of these chromatin marks was found across a broad array of immune cell types (Figure S5B). Pivotal roles of PRCs in transcription silencing and chromatin compaction have been extensively described (Margueron and Reinberg, 2011). Our data argue that the levels of chromatin marks directly mediated by PRCs become highly variable from cell to cell upon aging.

H3K27me3-Marked Genes Are Associated with Higher Transcriptional Variability with Age

Next, we tested if the increased instability of chromatin state with age is associated with elevated transcriptional noise (Raj and van Oudenaarden, 2008). Because single-cell RNA-seq (scRNA-seq) on an aging cohort with matching ChIP-seq data has not yet been described in humans, we performed analyses on a scRNA-seq dataset on naive CD4⁺ T cells purified from an inbred mouse strain (C57BL/6J, *M. musculus domesticus*), where Martinez-Jimenez et al. (2017) reported aging-associated increases in single-cell transcriptional variability. We analyzed the data in conjunction with a ChIP-seq dataset mapping H3K27me3 and H3K4me3 occupancies at genes with vital immune functions and critical roles in cell differentiation in naive CD4⁺ T cells purified from the same C57BL/6J substrain (Wei et al., 2009). Our EpiTOF data showed that single-cell variability in H3K4me3 is not altered significantly with age across several immune cell subtypes (Figure S5C). To test the relationship between noise in chromatin marks and noise in transcription, we compared the

(C) Differential chromatin marks in regulatory T cells. Heatmap representation of the effect sizes of the levels of 40 chromatin marks in Tregs over total CD4⁺ T cells in the indicated biological replicates.

(D and E) Differential chromatin marks separate CD56^{bright} NK cells from the CD56^{dim} subset. Scatterplot of single-cell EpiTOF data from NK cells (bio rep 1). Each dot represents a single NK cell plotted based on CD56 (y axis) and CD16 (x axis) levels. Color, PC1 computed from the 20 chromatin marks measured by EpiTOF panel 1. Density plot of the two populations segregated by MixTool (green, CD56^{bright}; red, CD56^{dim}) using CD56 level is shown (D). Heatmap representation of the effect sizes computed for the levels of the indicated chromatin marks in CD56^{bright} over CD56^{dim} subsets. Data from both biological replicates are shown (E). See also Figure S3 and Table S3.

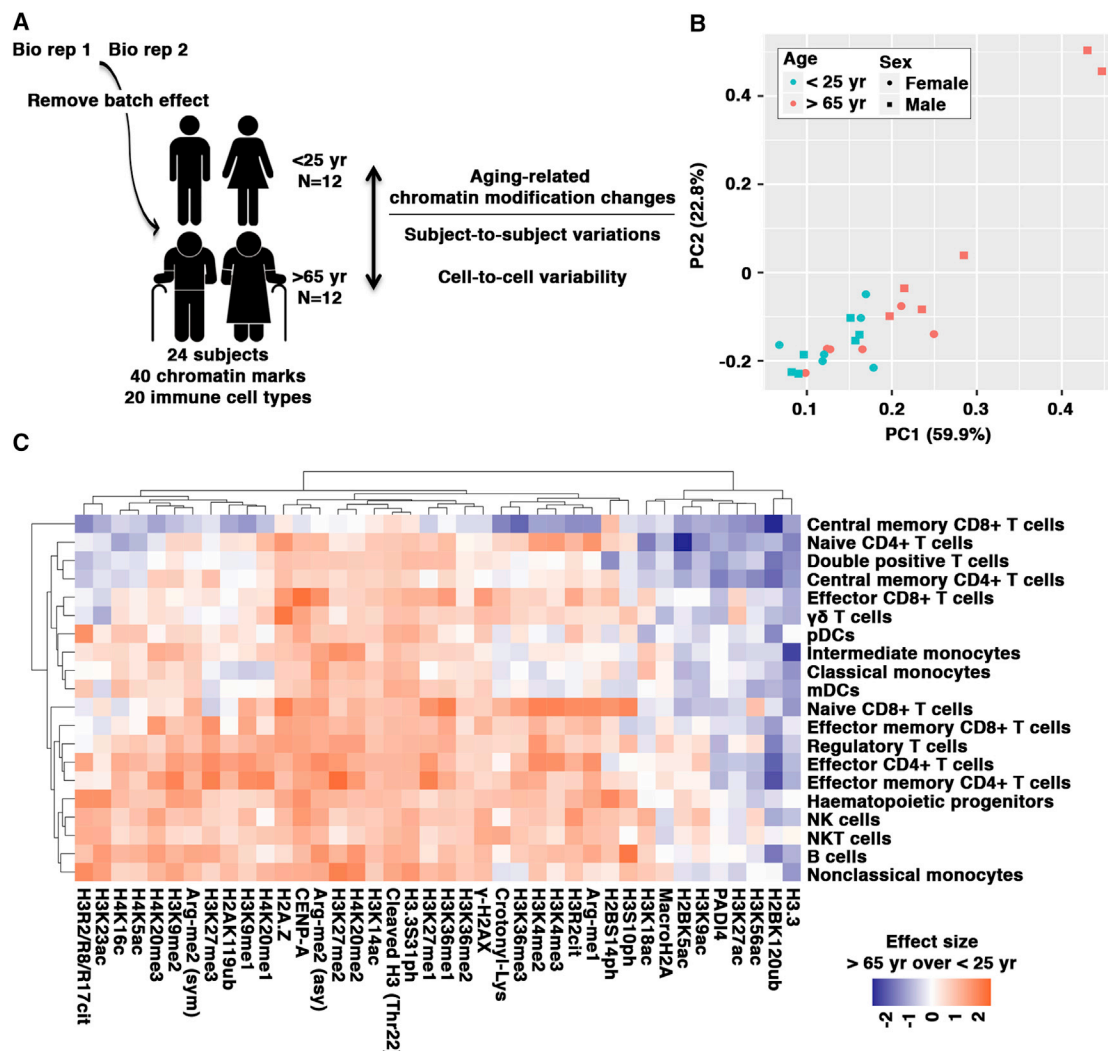


Figure 4. Increased Variations in Chromatin Modification Profiles with Age

(A) Data integration for aging-related analyses. Two biological replicates are merged using empirical Bayes framework to correct for batch effect. Data collected from 9 major immune cell types in the initial EpiTOF analysis (Figures 1C and S1A; exclude total CD4⁺ and CD8⁺ T cells) are integrated with data from 11 T cell subsets (Figures 3A and S3A) to create a dataset of 40 chromatin marks in 20 immune cell subsets (800 data points) for each of the 24 subjects.

(B) Increased subject-to-subject variability with aging. PCA of EpiTOF data from 24 healthy subjects described in (A) (salmon, >65 years; cyan, <25 years; circle, female; square, male). Each dot represents a single subject situated in the PCA plot, where each principal component summarizes the variance of 800 data points. The percentage of variance each principal component explains is shown.

(C) Aging is associated with alterations of a broad range of chromatin marks. Heatmap representation of the effect sizes of the levels of the indicated chromatin mark (x axis) and immune cell type (y axis) pairs in older over younger subjects. Dendrogram, unsupervised clustering.

See also Figure S4.

transcriptional noise of H3K27me3-marked genes with the genes enriched with H3K4me3. Between both datasets, we identified 43 genes marked by H3K27me3 (without H3K4me3) and 210 with H3K4me3 (without H3K27me3). We found that H3K27me3-marked genes are largely repressed, while H3K4me3-marked genes are actively transcribed (Figure S5D), indicating that the gene expression activities measured by both independent studies are highly comparable. Importantly, the selected genes were not differentially expressed between young and old mice (Figure S5D), allowing us to directly compare transcriptional noise between both age groups. We found that genes enriched

with H3K27me3 showed significantly higher transcriptional variability with age than genes marked by H3K4me3 (Figure 5C). Our data suggest a model in which elevated epigenomic noise, in particular PRC-mediated H3K27me3, results in variations in chromatin states between single cells and ultimately leads to higher transcriptional noise during aging.

Variations in the Chromatin Modification Profiles Are Largely Driven by Non-heritable Influences

Our earlier work indicating that the vast majority (77%) of variables in the human immune system are driven by non-heritable

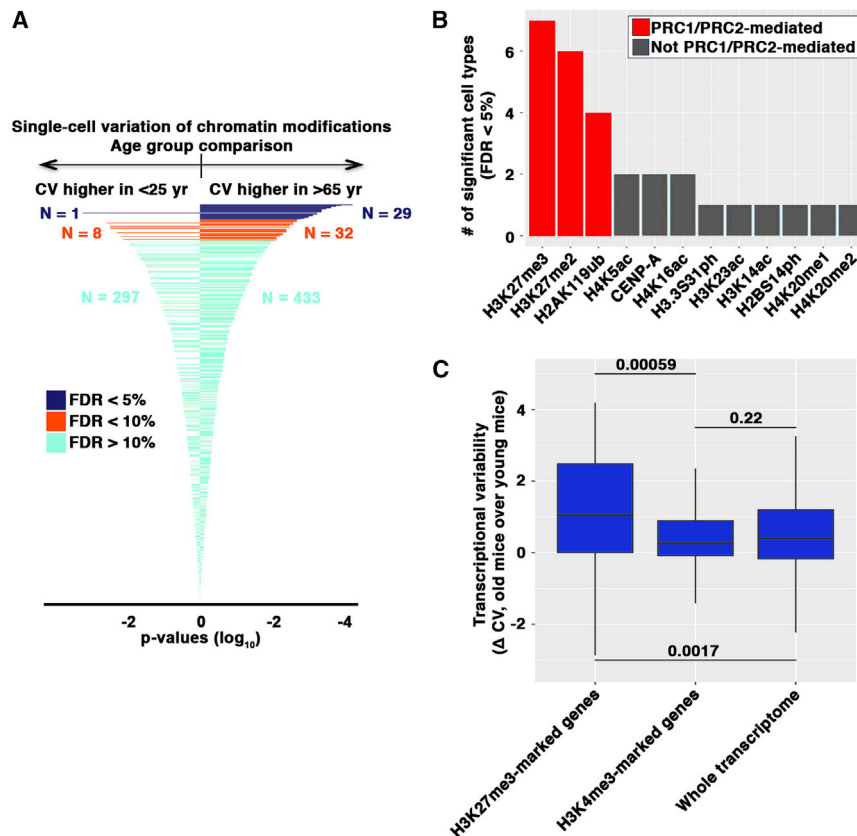


Figure 5. Cell-to-Cell Variability of Chromatin Modification Profiles Increases with Age

(A) Aging is associated with elevated single-cell variations in chromatin modifications. t test comparison of the CVs of 800 data points between subjects from the two age groups. x axis, p values; directionality, CV higher in subjects <25 years (left) or higher in subject >65 years (right); color, FDR (dark blue, <5%; orange, 5%–10%; light blue, >10%). Test results are ranked by FDRs from top to bottom.

(B) H3K27me2, H3K27me3, and H2AK119ub show the greatest increase in cell-to-cell variability with age. The numbers of immune cell types (y axis) in which the indicated chromatin marks (x axis) show statistically significant (FDR < 5%) increase in CVs in older subjects. Red, chromatin marks generated by PRC1 or PRC2; gray, chromatin marks that are not catalyzed by PRCs.

(C) H3K27me3-marked genes are associated with increased cell-to-cell transcriptional variability with age. Changes in transcriptional variability (ΔCV) between naive CD4⁺ T cells purified from old and young *M. musculus domesticus* of the indicated gene subsets are computed. Transcription profiling data and lists of genes occupied by H3K27me3 or H3K4me3 are derived from publicly available scRNA-seq (Martinez-Jimenez et al., 2017) and ChIP-seq (Wei et al., 2009) datasets, respectively. Transcriptome-wide increased transcriptional noise with age is shown. p values, Wilcoxon's paired rank-sum test.

See also Figure S5.

influences (Brodin et al., 2015) led us to postulate that environmental and/or other non-heritable factors are the primary driving force for variations in chromatin modification profiles in immune cells. We conducted EpiTOF analysis using both the broad immune cell EpiTOF panels and the T-cell-focused panels on a cohort of 9 pairs of monozygotic (MZ) and 10 pairs of dizygotic (DZ) twins selected from the twin registry described in the Brodin et al. (2015) study. All subjects were CMV-seronegative and either between 15 and 29 (younger twins) or 52 and 72 (older twins) in age (Figure 6A). We analyzed data utilizing the classical ACE model, which calculates the fractions of variance attributed to additive genetics (A), common environment (C) or unique environment (E) (Rijsdijk and Sham, 2002). Non-heritable factors explain 70% of the variance in chromatin modifications in immune cells, whereas genetics accounts for 30% of the variance (Figure 6B). Within non-heritable factors, shared and unique environment explain 13.5% and 56.5% of the variance, respectively. While largely driven by non-heritable influences, genetic contributions to the variance are not trivial. Specifically, CD45RO⁺CCR7⁺ naive, CD45RO⁺CCD7⁺ central memory and CD45RO⁺CCD7[−] effector memory CD4⁺ T cells, whose frequencies in the CD4⁺ T cell compartment are driven significantly by heritable factors (Brodin et al., 2015), were among the top cell subsets in which genetics showed prominent influences on chromatin marks (Figure 6B). Together, our results indicate that the variance in chromatin modification profiles is largely driven by non-heritable influences, with considerable contributions from genetic influences.

Divergence of Chromatin Modification Profiles between Genetically Related Twins Widens with Age

We next investigate our discoveries of aging-associated phenotypes at chromatin in the twin cohort. Consistent with our findings in Figure 4C, the vast majority of the chromatin marks were elevated in older twin subjects (Figure S6A). We further observed globally repressed chromatin marks in central memory CD8⁺ T cells with age (Figure S6A). We also found that 68.8% of the 800 chromatin mark- and cell-type pairs showed higher CVs in older twins (Figure S6B). Collectively, our findings from the independent twin cohort confirm and extend our earlier findings.

Next, we performed PCA on the twin subjects based on 800 data points. PC1 and PC2, which together explained 92.7% of the variance in the dataset, showed increased heterogeneity between older twin pairs (Figure 6C). Euclidean distances based on 800 data points between each twin pair revealed that older twins (Figure 6D, left) and randomly selected genetically unrelated older subjects (Figure 6D, right) showed higher heterogeneity in chromatin modification profiles, indicating that increased variations in chromatin modification profiles with age are largely driven by non-heritable influences. Younger MZ twins are more concordant in chromatin marks than DZ twins and randomly paired subjects (Figure 6E, top), suggesting the importance of additive genetics and/or the epigenome in zygotes in determining chromatin modification profiles in early life. However, Euclidean distances between older twins, both MZ and DZ, are indistinguishable from randomly paired subjects (Figure 6E,

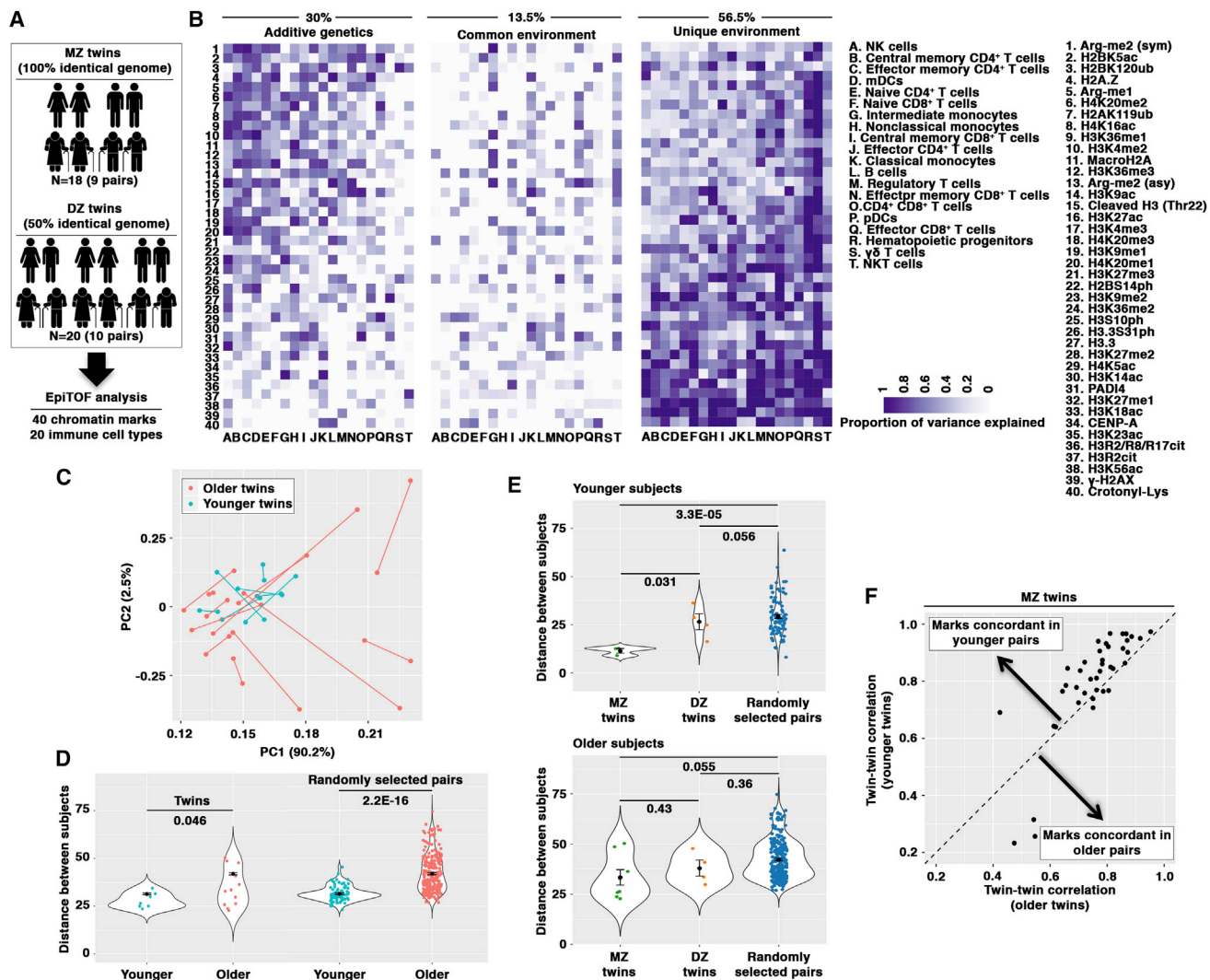


Figure 6. Non-heritable Influences Explain Most Variations in Chromatin Modification Profiles

(A) Overview of heritability analyses. Nine pairs of monozygotic (MZ) twins and ten pairs of dizygotic (DZ) twins were subjected to EpiTOF analysis utilizing four EpiTOF panels covering major immune cells and T cell subsets.

(B) Variance in chromatin modification profiles is largely driven by unique environmental factors. Heatmap representation of the proportions of variance explained by additive genetics (left), common environment (middle), or unique environment (right) for the indicated chromatin mark and immune cell subset pairs. Chromatin marks are ranked from top to bottom based on the average influences from additive genetics. Immune cells are ranked from left to right by the averages of additive genetics influences across all chromatin marks. The average influences of each component on all 800 data points are shown.

(C and D) Aging is associated with divergent chromatin modification profiles between twins. PCA of younger (cyan) and older (salmon) twin subjects. Each dot represents a single twin subject, and the twins are connected. Principal component, variance of 800 data points. The percentage of variance explained by each principal component is shown (C). Euclidean distances of 800 chromatin mark- and cell-type pairs are computed for each pair of twins (left) or randomly selected genetically unrelated subjects (right) from separate age groups (cyan, younger subjects; salmon, older subjects). p values for the statistical significance of increased Euclidean distance in older pairs are shown (D). Error bars, SE.

(E) Concordance of chromatin modification profiles in younger MZ twins diminishes with age. Euclidean distances calculated from the 800 data points between MZ (left), DZ (middle) twins, and randomly paired genetically unrelated individuals (right). Top, younger subjects; bottom, older subjects. p values for the statistical significance of distinct Euclidean distance are shown. Error bars, SE.

(F) Non-heritable influences drive the increased variability in chromatin modifications with age. Spearman's rank correlations of 40 chromatin marks across 20 immune cell types are computed for younger and older MZ twins. Each dot represents a chromatin mark. x axis, correlation between older twin pairs; y axis, correlation between young twin pairs. Dashed line, equal correlation in younger and older MZ twins. Arrows indicate the directions of higher concordance in younger pairs (upper left) or in older pairs (lower right).

See also Figure S6.

bottom), suggesting impacts of environmental influences and/or somatic mutations accumulated through the lifetime of an individual on chromatin modifications. To further strengthen our findings, the concordance of 32 of the 40 chromatin marks in MZ twins, where genetics and the epigenome in zygotes are completely controlled, was higher between younger pairs than older pairs (Figure 6F), underscoring the prominent effects of non-heritable influences on the variation of chromatin marks between individuals.

DISCUSSION

In this study we present a mass cytometry-based analytical platform focusing on epigenetic markers that is broadly applicable to several areas of chromatin and immunology research. The versatility of EpiTOF can be seen by the fact that different immunophenotypic markers can be used to interrogate unique immune cells (e.g., antigen-specific T cells) or single-cell suspensions derived from solid tissues, such as skin, kidney, and synovium. Next, EpiTOF can be employed to identify chromatin marks dysregulated in immune-mediated diseases, cancer, and other human conditions to facilitate the development of therapeutic agents targeting chromatin modifying enzymes.

The process of aging is known to involve multiple genes and pathways and, importantly, epigenetic regulation (Benayoun et al., 2015; Dorshkind et al., 2009). In this study we report a number of epigenetic signatures at chromatin associated with aging in human immune cells. Variations of chromatin modification profiles between individuals increase with age, suggesting that aging does not affect chromatin marks uniformly with time. While variations increase between individuals, we observe elevations of most chromatin marks with age across three independent cohorts. Consistent increases in chromatin marks in a broad array of cell subtypes from hematopoietic progenitors to terminally differentiated immune cells suggests that systemic changes may result from the reprogrammed chromatin state in hematopoietic progenitors or further upstream in hematopoietic stem cells (HSCs). Our findings are in agreement with a comprehensive study showing increases in both H3K4me3 and H3K27me3 marks in murine HSCs from old mice (Sun et al., 2014). We extend this observation to a broad array of chromatin marks and show that the increases are not due to histone loss.

Importantly, we demonstrate that increased cell-to-cell variability in chromatin modifications within each immune cell subtype is a molecular signature of aging. Elevated single-cell transcriptional variability with age has been reported in several studies (Bahar et al., 2006; Enge et al., 2017; Martinez-Jimenez et al., 2017); however, the molecular mechanisms underlying the transcriptional variability remain unclear. Our data suggest a compelling model in which increased epigenomic noise, which we define by single-cell variability in chromatin marks, is a major mechanism that results in elevated transcriptional noise with age. While the origins of increased epigenomic noise with age remain to be defined, it is possible that the variability arises from distinct clones of HSCs from which immune cells are derived, and the chromatin modification profiles of independent clones of HSCs diverges with age. In addition, the discoveries of increased variability of PRC-mediated repressive chromatin

marks with age and higher transcriptional noise of H3K27me3-target genes further strengthen the links between epigenomic noise and single-cell transcriptional variability. Sporadic loss of silencing of transcriptionally inactive genes may be one of the molecular mechanisms that results in changes in gene expression programs with age. Transient reactivation of certain genes may confer growth advantages to cells and result in long-term transcriptional alterations.

Finally, our data from the twin cohort show that the variations in chromatin marks are predominantly driven by non-heritable influences (70%). Increased variations in chromatin marks between twin pairs in older MZ twins further suggest that environmental influences play a key role in the divergence. However, our results also find considerable involvement of heritable factors (30%). Our findings are highly similar to results from twin analyses on DNA methylation, where environmental influences explain approximately 80% of the variance in DNA methylation (McRae et al., 2014; van Dongen et al., 2016). Closer concordance in MZ twins than in DZ twins in DNA methylation suggests that heritable influences are not trivial (Kaminsky et al., 2009). It has been proposed that MZ twins start with identical epigenomes in the zygotes and, therefore, remain more similar to each other than DZ twins, who develop from independent zygotes with distinct epigenomes (Petronis, 2010). This hypothesis helps explain our results on chromatin modifications in twins; however, a unified mechanism for the patterns of chromatin modifications to be re-established during mitotic cell division remains unclear (Zhu and Reinberg, 2011). Our data highlight the importance of identifying the molecular mechanisms by which chromatin marks are inherited through cell cycle and possibly through generations.

STAR★METHODS

Detailed methods are provided in the online version of this paper and include the following:

- KEY RESOURCES TABLE
- CONTACT FOR REAGENT AND RESOURCE SHARING
- EXPERIMENTAL MODEL AND SUBJECT DETAILS
 - Human Subjects
- METHOD DETAILS
 - PBMC Isolation
 - Lanthanide Labeling of Antibodies for Mass Cytometry
 - Mass Cytometry (Sample Processing, Staining, Bar-coding and Data Collection)
 - Immune Cell Population Definitions (Gating Strategies) and Data Pre-Processing
 - FACS and Western Blotting
 - Data processing, normalization, and visualization
 - Integrated ChIP-seq and transcriptional analysis of lymphoid and myeloid cells (Figures 1E and 1F)
 - Classification of immune cell type using chromatin marks (Figures 2A–2C)
 - Single-cell analysis of the relationship between chromatin mark pairs (Figure 2D)
 - Discovery of chromatin-defined cell subsets in NK cells (Figure 3)
 - Subject-level analysis of chromatin profiles (Figure 4)

- Quantification of cell-to-cell variation in chromatin levels (Figure 5)
- Heritability analysis of the twin cohort (Figure 6)
- List of R packages

SUPPLEMENTAL INFORMATION

Supplemental Information includes six figures, three tables, and two data files and can be found with this article online at <https://doi.org/10.1016/j.cell.2018.03.079>.

ACKNOWLEDGMENTS

We thank Drs. Catherine Blish, Anne Brunet, Or Gozani, and Robin Yeo (alphabetically listed) for insightful discussions. We thank the Stanford Blood Center and LPCH Vaccine Program staff for recruiting subjects and collecting blood samples. We thank Dr. Holden Maecker and Stanford Human Immune Monitoring Center (HIMC) for coordinating the selection of twin samples from Cooperative Center for Human Immunology (funded by U19AI057229) (to M.M.D.). We thank the Stanford Shared FACS Facility (SSFF), where cell sorting, flow cytometry, and CyTOF were performed. The instruments at SSFF were made possible in part by NIH funding (S10RR025518-01, S10RR027431-01, and S10OD016318-01). This work was supported in part by grants from Autoimmunity Center of Excellence (5U19AI110491-04 and 5UM1A110498-04), a research consortium supported by the NIAID/NIH (to P.J.U.), the Bill & Melinda Gates Foundation (to P.K.), the Donald E. and Delia B. Baxter Foundation (to P.J.U.), Elizabeth F. Adler (to P.J.U.), the Henry Gustav Floren Trust (to P.J.U.), NIH (5U19AI109662-05) (to P.K.), NIH Clinical and Translational Science Award (UL1 RR025744) for the Stanford Center for Clinical and Translational Education and Research (Spectrum), NIH (5R01AI125197-02) (to P.J.U. and P.K.), NIH (5U19AI057229-15) (to P.K.), and NIH (U19AI090019) (to M.M.D.) (listed alphabetically). P.C. was supported by NIH T32 training grant 2T32AR050942-06A1 and Novo Nordisk Senior Postdoctoral Fellowship. F.V. was supported by NIH K12 Award 5K12HL120001-02. H.C.W. was supported by NIH T32 training grant 5T32AI07290-31. A.J.K. was supported by NIH T32 training grant 5T32AI007290-29 and Novo Nordisk Senior Postdoctoral Fellowship. ClinicalTrials.gov numbers for the studies that contributed twin participant samples are NCT01987349, NCT03022396, and NCT03022422.

AUTHOR CONTRIBUTIONS

P.C. and A.J.K. conceived of and established the methods for EpiTOF and performed experiments under the supervision of P.J.U.; F.V. conceived of the methods to analyze the EpiTOF data and performed analyses under the supervision of P.K.; H.C.W., M.D., S.S., S.E.C., and M.D. assisted with the experiments and the data analyses; C.L.D. was responsible for all regulatory and clinical aspects of the studies collecting samples from twin subjects and provided input with M.M.D. on the twin experiments; and P.C., F.V., P.J.U., P.K., and A.J.K. jointly designed the experiments, interpreted the results, and wrote the manuscript with contributions from all co-authors.

DECLARATION OF INTERESTS

The authors declare no competing interests.

Received: January 5, 2018

Revised: February 27, 2018

Accepted: March 28, 2018

Published: April 26, 2018

REFERENCES

Agaloti, T., Chen, G., and Thanos, D. (2002). Deciphering the transcriptional histone acetylation code for a human gene. *Cell* 111, 381–392.

Andres-Terre, M., McGuire, H.M., Pouliot, Y., Bongen, E., Sweeney, T.E., Tato, C.M., and Khatri, P. (2015). Integrated, multi-cohort analysis identifies

conserved transcriptional signatures across multiple respiratory viruses. *Immunity* 43, 1199–1211.

Arvey, A., van der Veecken, J., Samstein, R.M., Feng, Y., Stamatoyannopoulos, J.A., and Rudensky, A.Y. (2014). Inflammation-induced repression of chromatin bound by the transcription factor Foxp3 in regulatory T cells. *Nat. Immunol.* 15, 580–587.

Bahar, R., Hartmann, C.H., Rodriguez, K.A., Denny, A.D., Busuttill, R.A., Dollé, M.E., Calder, R.B., Chisholm, G.B., Pollock, B.H., Klein, C.A., and Vijg, J. (2006). Increased cell-to-cell variation in gene expression in ageing mouse heart. *Nature* 441, 1011–1014.

Barski, A., Cuddapah, S., Cui, K., Roh, T.Y., Schones, D.E., Wang, Z., Wei, G., Chepelev, I., and Zhao, K. (2007). High-resolution profiling of histone methylations in the human genome. *Cell* 129, 823–837.

Benaglia, T., Chauveau, D., Hunter, D.R., and Young, D.S. (2009). mixtools: an R package for analyzing finite mixture models. *J. Stat. Softw.* 32, 1–29.

Benayoun, B.A., Pollina, E.A., and Brunet, A. (2015). Epigenetic regulation of ageing: linking environmental inputs to genomic stability. *Nat. Rev. Mol. Cell Biol.* 16, 593–610.

Bendall, S.C., Simonds, E.F., Qiu, P., Amir, A.D., Krutzik, P.O., Finck, R., Bruggner, R.V., Melamed, R., Trejo, A., Ornatsky, O.I., et al. (2011). Single-cell mass cytometry of differential immune and drug responses across a human hematopoietic continuum. *Science* 332, 687–696.

Bernstein, B.E., Stamatoyannopoulos, J.A., Costello, J.F., Ren, B., Milosavljevic, A., Meissner, A., Kellis, M., Marra, M.A., Beaudet, A.L., Ecker, J.R., et al. (2010). The NIH Roadmap Epigenomics Mapping Consortium. *Nat. Biotechnol.* 28, 1045–1048.

Booth, L.N., and Brunet, A. (2016). The aging epigenome. *Mol. Cell* 62, 728–744.

Brodin, P., and Davis, M.M. (2017). Human immune system variation. *Nat. Rev. Immunol.* 17, 21–29.

Brodin, P., Jovic, V., Gao, T., Bhattacharya, S., Angel, C.J., Furman, D., Shen-Orr, S., Dekker, C.L., Swan, G.E., Butte, A.J., et al. (2015). Variation in the human immune system is largely driven by non-heritable influences. *Cell* 160, 37–47.

Buenrostro, J.D., Wu, B., Litzenburger, U.M., Ruff, D., Gonzales, M.L., Snyder, M.P., Chang, H.Y., and Greenleaf, W.J. (2015). Single-cell chromatin accessibility reveals principles of regulatory variation. *Nature* 523, 486–490.

Chien, Y.H., Meyer, C., and Bonneville, M. (2014). $\gamma\delta$ T cells: first line of defense and beyond. *Annu. Rev. Immunol.* 32, 121–155.

Cooper, M.A., Fehniger, T.A., Turner, S.C., Chen, K.S., Ghaehri, B.A., Ghayur, T., Carson, W.E., and Caligiuri, M.A. (2001). Human natural killer cells: a unique innate immunoregulatory role for the CD56(bright) subset. *Blood* 97, 3146–3151.

Corces, M.R., Buenrostro, J.D., Wu, B., Greenside, P.G., Chan, S.M., Koenig, J.L., Snyder, M.P., Pritchard, J.K., Kundaje, A., Greenleaf, W.J., et al. (2016). Lineage-specific and single-cell chromatin accessibility charts human hematopoiesis and leukemia evolution. *Nat. Genet.* 48, 1193–1203.

Cover, T.M., and Thomas, J.A. (2012). *Elements of Information Theory* (Wiley).

Cuthbert, G.L., Daujat, S., Snowden, A.W., Erdjument-Bromage, H., Hagiwara, T., Yamada, M., Schneider, R., Gregory, P.D., Tempst, P., Bannister, A.J., and Kouzarides, T. (2004). Histone deimination antagonizes arginine methylation. *Cell* 118, 545–553.

Di Croce, L., and Helin, K. (2013). Transcriptional regulation by Polycomb group proteins. *Nat. Struct. Mol. Biol.* 20, 1147–1155.

Dorshkind, K., Montecino-Rodriguez, E., and Signer, R.A. (2009). The ageing immune system: is it ever too old to become young again? *Nat. Rev. Immunol.* 9, 57–62.

DuPage, M., Chopra, G., Quiros, J., Rosenthal, W.L., Morar, M.M., Holohan, D., Zhang, R., Turka, L., Marson, A., and Bluestone, J.A. (2015). The chromatin-modifying enzyme Ezh2 is critical for the maintenance of regulatory T cell identity after activation. *Immunity* 42, 227–238.

Engel, M., Arda, H.E., Mignardi, M., Beausang, J., Bottino, R., Kim, S.K., and Quake, S.R. (2017). Single-cell Analysis of Human Pancreas Reveals

Transcriptional Signatures of Aging and Somatic Mutation Patterns. *Cell* 171, 321–330.e314.

Friedman, J.H., Hastie, T., and Tibshirani, R. (2010). Regularization Paths for Generalized Linear models via Coordinate Descent. *J. Stat. Softw.* 33, 1–22.

Gomez, D., Shankman, L.S., Nguyen, A.T., and Owens, G.K. (2013). Detection of histone modifications at specific gene loci in single cells in histological sections. *Nat. Methods* 10, 171–177.

Hu, H., Wang, B., Borde, M., Nardone, J., Maika, S., Allred, L., Tucker, P.W., and Rao, A. (2006). Foxp1 is an essential transcriptional regulator of B cell development. *Nat. Immunol.* 7, 819–826.

Johnson, W.E., Li, C., and Rabinovic, A. (2007). Adjusting batch effects in microarray expression data using empirical Bayes methods. *Biostatistics* 8, 118–127.

Kaczorowski, K.J., Shekhar, K., Nkulikiyimfura, D., Dekker, C.L., Maecker, H., Davis, M.M., Chakraborty, A.K., and Brodin, P. (2017). Continuous immunotypes describe human immune variation and predict diverse responses. *Proc. Natl. Acad. Sci. USA* 114, E6097–E6106.

Kaminsky, Z.A., Tang, T., Wang, S.C., Ptak, C., Oh, G.H., Wong, A.H., Feldcamp, L.A., Virtanen, C., Halfvarson, J., Tysk, C., et al. (2009). DNA methylation profiles in monozygotic and dizygotic twins. *Nat. Genet.* 41, 240–245.

Kouzarides, T. (2007). Chromatin modifications and their function. *Cell* 128, 693–705.

Lanier, L.L., Le, A.M., Civin, C.I., Loken, M.R., and Phillips, J.H. (1986). The relationship of CD16 (Leu-11) and Leu-19 (NKH-1) antigen expression on human peripheral blood NK cells and cytotoxic T lymphocytes. *J. Immunol.* 136, 4480–4486.

Li, Q., Zou, J., Wang, M., Ding, X., Chepelev, I., Zhou, X., Zhao, W., Wei, G., Cui, J., Zhao, K., et al. (2014). Critical role of histone demethylase Jmjd3 in the regulation of CD4+ T-cell differentiation. *Nat. Commun.* 5, 5780.

Love, M.I., Huber, W., and Anders, S. (2014). Moderated estimation of fold change and dispersion for RNA-seq data with DESeq2. *Genome Biol.* 15, 550.

Margueron, R., and Reinberg, D. (2011). The Polycomb complex PRC2 and its mark in life. *Nature* 469, 343–349.

Martinez-Jimenez, C.P., Eling, N., Chen, H.C., Vallejos, C.A., Kolodziejczyk, A.A., Connor, F., Stojic, L., Rayner, T.F., Stubbington, M.J.T., Teichmann, S.A., et al. (2017). Aging increases cell-to-cell transcriptional variability upon immune stimulation. *Science* 355, 1433–1436.

Maze, I., Noh, K.M., Soshnev, A.A., and Allis, C.D. (2014). Every amino acid matters: essential contributions of histone variants to mammalian development and disease. *Nat. Rev. Genet.* 15, 259–271.

Mazzucchelli, R., and Durum, S.K. (2007). Interleukin-7 receptor expression: intelligent design. *Nat. Rev. Immunol.* 7, 144–154.

McRae, A.F., Powell, J.E., Henders, A.K., Bowdler, L., Hemani, G., Shah, S., Painter, J.N., Martin, N.G., Visscher, P.M., and Montgomery, G.W. (2014). Contribution of genetic variation to transgenerational inheritance of DNA methylation. *Genome Biol.* 15, R73.

Moskowitz, D.M., Zhang, D.W., Hu, B., Le Saux, S., Yanes, R.E., Ye, Z., Buenrostro, J.D., Weyand, C.M., Greenleaf, W.J., and Goronzy, J.J. (2017). Epigenomics of human CD8 T cell differentiation and aging. *Sci. Immunol.* 2, 2.

Petronis, A. (2010). Epigenetics as a unifying principle in the aetiology of complex traits and diseases. *Nature* 465, 721–727.

Pevny, L., Simon, M.C., Robertson, E., Klein, W.H., Tsai, S.F., D'Agati, V., Orkin, S.H., and Costantini, F. (1991). Erythroid differentiation in chimaeric mice blocked by a targeted mutation in the gene for transcription factor GATA-1. *Nature* 349, 257–260.

Raj, A., and van Oudenaarden, A. (2008). Nature, nurture, or chance: stochastic gene expression and its consequences. *Cell* 135, 216–226.

Raser, J.M., and O'Shea, E.K. (2004). Control of stochasticity in eukaryotic gene expression. *Science* 304, 1811–1814.

Rijsdijk, F.V., and Sham, P.C. (2002). Analytic approaches to twin data using structural equation models. *Brief. Bioinform.* 3, 119–133.

Rogakou, E.P., Pilch, D.R., Orr, A.H., Ivanova, V.S., and Bonner, W.M. (1998). DNA double-stranded breaks induce histone H2AX phosphorylation on serine 139. *J. Biol. Chem.* 273, 5858–5868.

Rotem, A., Ram, O., Shores, N., Sperling, R.A., Goren, A., Weitz, D.A., and Bernstein, B.E. (2015). Single-cell ChIP-seq reveals cell subpopulations defined by chromatin state. *Nat. Biotechnol.* 33, 1165–1172.

Schwartzman, O., and Tanay, A. (2015). Single-cell epigenomics: techniques and emerging applications. *Nat. Rev. Genet.* 16, 716–726.

Scott, E.W., Simon, M.C., Anastasi, J., and Singh, H. (1994). Requirement of transcription factor PU.1 in the development of multiple hematopoietic lineages. *Science* 265, 1573–1577.

Shi, Y. (2007). Histone lysine demethylases: emerging roles in development, physiology and disease. *Nat. Rev. Genet.* 8, 829–833.

Sun, D., Luo, M., Jeong, M., Rodriguez, B., Xia, Z., Hannah, R., Wang, H., Le, T., Faull, K.F., Chen, R., et al. (2014). Epigenomic profiling of young and aged HSCs reveals concerted changes during aging that reinforce self-renewal. *Cell Stem Cell* 14, 673–688.

Talbert, P.B., and Henikoff, S. (2017). Histone variants on the move: substrates for chromatin dynamics. *Nat. Rev. Mol. Cell Biol.* 18, 115–126.

Taverna, S.D., Li, H., Ruthenburg, A.J., Allis, C.D., and Patel, D.J. (2007). How chromatin-binding modules interpret histone modifications: lessons from professional pocket pickers. *Nat. Struct. Mol. Biol.* 14, 1025–1040.

Trojer, P., and Reinberg, D. (2007). Facultative heterochromatin: is there a distinctive molecular signature? *Mol. Cell* 28, 1–13.

Turner, C.A., Jr., Mack, D.H., and Davis, M.M. (1994). Blimp-1, a novel zinc finger-containing protein that can drive the maturation of B lymphocytes into immunoglobulin-secreting cells. *Cell* 77, 297–306.

Ucar, D., Márquez, E.J., Chung, C.H., Marches, R., Rossi, R.J., Uyar, A., Wu, T.C., George, J., Stitzel, M.L., Palucka, A.K., et al. (2017). The chromatin accessibility signature of human immune aging stems from CD8⁺T cells. *J. Exp. Med.* 214, 3123–3144.

van Dongen, J., Nivard, M.G., Willemsen, G., Hottenga, J.J., Helmer, Q., Dolan, C.V., Ehli, E.A., Davies, G.E., van IJterson, M., Breeze, C.E., et al.; BIOS Consortium (2016). Genetic and environmental influences interact with age and sex in shaping the human methylome. *Nat. Commun.* 7, 11115.

Wagner, E.J., and Carpenter, P.B. (2012). Understanding the language of Lys36 methylation at histone H3. *Nat. Rev. Mol. Cell Biol.* 13, 115–126.

Wang, H., Wang, L., Erdjument-Bromage, H., Vidal, M., Tempst, P., Jones, R.S., and Zhang, Y. (2004a). Role of histone H2A ubiquitination in Polycomb silencing. *Nature* 431, 873–878.

Wang, Y., Wysocka, J., Sayegh, J., Lee, Y.H., Perlin, J.R., Leonelli, L., Sonbuchner, L.S., McDonald, C.H., Cook, R.G., Dou, Y., et al. (2004b). Human PAD4 regulates histone arginine methylation levels via demethyliminination. *Science* 306, 279–283.

Wei, G., Wei, L., Zhu, J., Zang, C., Hu-Li, J., Yao, Z., Cui, K., Kanno, Y., Roh, T.Y., Watford, W.T., et al. (2009). Global mapping of H3K4me3 and H3K27me3 reveals specificity and plasticity in lineage fate determination of differentiating CD4⁺ T cells. *Immunity* 30, 155–167.

Wertheimer, A.M., Bennett, M.S., Park, B., Uhrhlaib, J.L., Martinez, C., Pulko, V., Currier, N.L., Nikolich-Zugich, D., Kaye, J., and Nikolich-Zugich, J. (2014). Aging and cytomegalovirus infection differentially and jointly affect distinct circulating T cell subsets in humans. *J. Immunol.* 192, 2143–2155.

Wu, C., Li, B., Lu, R., Koelle, S.J., Yang, Y., Jares, A., Krouse, A.E., Metzger, M., Liang, F., Loré, K., et al. (2014). Clonal tracking of rhesus macaque hematopoiesis highlights a distinct lineage origin for natural killer cells. *Cell Stem Cell* 14, 486–499.

Zhang, D.E., Zhang, P., Wang, N.D., Hetherington, C.J., Darlington, G.J., and Tenen, D.G. (1997). Absence of granulocyte colony-stimulating factor signaling and neutrophil development in CCAAT enhancer binding protein alpha-deficient mice. *Proc. Natl. Acad. Sci. USA* 94, 569–574.

Zhu, B., and Reinberg, D. (2011). Epigenetic inheritance: uncontested? *Cell Res.* 21, 435–441.

STAR★METHODS

KEY RESOURCES TABLE

REAGENT or RESOURCE	SOURCE	IDENTIFIER
Antibodies		
Rabbit monoclonal anti-Histone H3 (clone D1H2)	Cell Signaling Technology	4499 (custom formulation*)
Rabbit monoclonal anti-phospho-Histone H2A.X (Ser139) (clone 20E3)	Cell Signaling Technology	9718 (custom formulation*)
Rabbit monoclonal anti-acetyl-Histone H2B (Lys5) (clone D5H1S)	Cell Signaling Technology	12799 (custom formulation*)
Mouse monoclonal anti-phospho-Histone H3 (Ser10) (clone MAB1 0312)	Active Motif	39636
Mouse monoclonal anti-acetyl-Histone H4 (Lys5) (clone MAB1 0405)	Active Motif	61523
Rabbit monoclonal anti-cleaved-Histone H3 (Thr22) (clone D7J2K)	Cell Signaling Technology	12576 (custom formulation*)
Mouse monoclonal anti-phospho-Histone H3.3 (Ser31) (clone 1A8G10)	Active Motif	61671
Rabbit monoclonal anti-acetyl-Histone H3 (Lys23) (clone RM169)	RevMAb Biosciences	31-1087-00 (custom formulation*)
Mouse monoclonal anti-acetyl-Histone H3 (Lys9) (clone 2G1F9)	Active Motif	61663
Rabbit monoclonal anti-phospho-Histone H2B (Ser14) (clone D67H2)	Cell Signaling Technology	6959 (custom formulation*)
Rabbit monoclonal anti-ubiquityl-Histone H2A (Lys119) (clone D27C4)	Cell Signaling Technology	8240 (custom formulation*)
Rabbit monoclonal anti-acetyl-Histone H3 (Lys18) (clone RM166)	RevMAb Biosciences	31-1055-00 (custom formulation*)
Mouse monoclonal anti-acetyl-Histone H3 (Lys56) (clone 12.1)	Active Motif	61061
Mouse monoclonal anti-peptidylarginine deiminase 4 (PADI4) (clone OT14H5)	OriGene	CF504813
Rabbit monoclonal anti-ubiquityl-Histone H2B (Lys120) (clone D11)	Cell Signaling Technology	5546 (custom formulation*)
Mouse monoclonal anti-crotonyllysine (clone 4D5)	PTM Biolabs	PTM-502
Rabbit monoclonal anti-citrullinated-Histone H3 (Arg2) (clone EPR17703)	abcam	ab176843
Rabbit monoclonal anti-acetyl-Histone H3 (Lys14) (clone D4B9)	Cell Signaling Technology	7627 (custom formulation*)
Rabbit polyclonal anti-citrullinated-Histone H3 (Arg2/8/17)	abcam	ab5103 (lot GR276206-1)
Rabbit monoclonal anti-acetyl-Histone H4 (Lys16) (clone E2B8W)	Cell Signaling Technology	13534 (custom formulation*)
Mouse monoclonal anti-Histone H4 (clone 31830)	abcam	ab31830
Mouse monoclonal anti-acetyl-Histone H3 (Lys27) (clone MAB1 0309)	Active Motif	39685
Mouse monoclonal anti-monomethylarginine (MMA) (clone 5D1)	abcam	ab415
Rabbit monoclonal antisymmetric dimethylarginine (SDMA)	Cell Signaling Technology	13222 (custom formulation*)
Mouse monoclonal anti-dimethyl-Histone H3 (Lys4) (clone MAB1 0303)	Active Motif	39679
Mouse monoclonal anti-dimethyl-Histone H3 (Lys9) (clone 5E5-G5)	BioLegend	815501
Mouse monoclonal anti-monomethyl-Histone H3 (Lys9) (clone 7E7.H12)	BioLegend	824201
Rabbit monoclonal anti-trimethyl-Histone H3 (Lys36) (clone RM155)	RevMAb Biosciences	31-1051-00 (custom formulation*)
Mouse monoclonal anti-monomethyl-Histone H3 (Lys27) (clone MAB1 0321)	Active Motif	61015
Rabbit monoclonal anti-asymmetric dimethylarginine (ADMA)	Cell Signaling Technology	13522 (custom formulation*)
Mouse monoclonal anti-dimethyl-Histone H3 (Lys36) (clone MAB1 0332)	Active Motif	61019
Mouse monoclonal anti-dimethyl-Histone H3 (Lys27) (clone MAB1 0324)	Active Motif	61435
Mouse monoclonal anti-dimethyl-Histone H4 (Lys20) (clone MAB1 0422)	Active Motif	61533
Rabbit monoclonal anti-Histone H3.3 (clone EPR17899)	abcam	ab176840
Mouse monoclonal anti-trimethyl-Histone H4 (Lys20) (clone 6F8-D9)	BioLegend	827701
Mouse monoclonal anti-macroH2A (clone 14G7)	Millipore	MABE61
Mouse monoclonal anti-trimethyl-Histone H3 (Lys4) (clone G.532.8)	ThermoFisher	MA5-11199 (custom formulation*)
Rabbit monoclonal anti-Histone H2A.Z (clone EPR6171(2)(B))	abcam	ab150402
Rabbit monoclonal anti-monomethyl-Histone H3 (Lys36) (clone EPR16993)	abcam	ab176920
Mouse monoclonal anti-trimethyl-Histone H3 (Lys27) (clone MAB1 0323)	Active Motif	61017
Mouse monoclonal anti-monomethyl-Histone H4 (Lys20) (clone 5E10-D8)	BioLegend	828001
Mouse monoclonal anti-CENP-A (clone 3-19)	MBL	D115-3
Mouse monoclonal anti-human CD45- ⁸⁹ Y (clone HI30)	Fluidigm	3089003B

(Continued on next page)

Continued

REAGENT or RESOURCE	SOURCE	IDENTIFIER
Mouse monoclonal anti-human CD4 (clone RPA-T4)	BioLegend	300541
Mouse monoclonal anti-human CD8 (clone SK1)	BioLegend	344727
Mouse monoclonal anti-human CD34 (clone 8G12)	BD	348050 (custom formulation*)
Mouse monoclonal anti-human CD11c (clone Bu15)	BioLegend	337221
Mouse monoclonal anti-human CD14 (clone M5E2)	BioLegend	301843
Mouse monoclonal anti-human CD33 (clone WM53)	BioLegend	303419
Mouse monoclonal anti-human CD16 (clone B73.1)	BioLegend	360702
Mouse monoclonal anti-human CD123 (clone 9F5)	BD	555642
Mouse monoclonal anti-human CD3 (clone UCHT1)	BioLegend	300443
Mouse monoclonal anti-human CD38 (clone HIT2)	BioLegend	303535
Mouse monoclonal anti-human CD56 (clone NCAM16.2)	BD	559043
Mouse monoclonal anti-human CD19 (clone HIB19)	BioLegend	302247
Mouse monoclonal anti-human HLA-DR (clone L243)	BioLegend	307651
Mouse monoclonal anti-human IL-17A (clone BL168)	BioLegend	512331
Mouse monoclonal anti-human TCR γ/δ (clone B1)	BioLegend	331202
Mouse monoclonal anti-human CD197 (CCR7) (clone G043H7)	BioLegend	353237
Mouse monoclonal anti-human CD294 (CRTH2) (clone BM16)	BioLegend	350102
Mouse monoclonal anti-human CD45RO (clone UCHL1)	BioLegend	304239
Mouse monoclonal anti-human TBX21 (T-bet) (clone 4B10)	BioLegend	644825
Mouse monoclonal anti-human FOXP3 (clone 259D/C7)	BD	560044
FITC-mouse monoclonal anti-human CD45 (clone HI30)	BioLegend	304038
PE/Cy7-mouse monoclonal anti-human CD3 (clone UCHT1)	BioLegend	300420
Alexa Fluor 647-mouse monoclonal anti-human CD19 (clone HIB19)	BioLegend	302220
PE-mouse monoclonal anti-human CD14 (clone M5E2)	BioLegend	301806
FITC-mouse monoclonal anti-human CD56 (clone NCAM16.2)	BD	340723
Rabbit monoclonal anti-neutrophil elastase (clone EPR7479)	abcam	ab131260
Rabbit monoclonal anti-lambda light chain (clone RM127)	RevMAb Biosciences	31-1029-00
Rabbit polyclonal anti-granzyme B	Cell Signaling Technology	4275S
* Custom formulation: PBS, > 1mg/mL, carrier-free, azide-free.		
Biological Samples		
Buffy coat from whole blood (for bio rep 1 and 2)	Stanford Blood Center	https://bloodcenter.stanford.edu/research-labs/research-products-and-services/blood-products/
PBMCs from twin subjects	Brodin et al. (2015) study (PMID: 25594173)	http://www.cell.com/cell/fulltext/S0092-8674(14)01590-6
Chemicals, Peptides, and Recombinant Proteins		
Ficoll-Paque PLUS	GE Healthcare	17-1440-02
RBC lysis buffer (10X)	BioLegend	420301
DMSO	Sigma	D2650
TCEP	ThermoFisher	77720
Sodium azide	Sigma	S2002
EDTA	Fisher	BP120-500
16% paraformaldehyde	Electron Microscopy Sciences	15710
Methanol	Fisher Scientific	A454-4
PBS	ThermoFisher	10010-072
Software and Algorithms		
FlowJo	FlowJo, LLC	https://www.flowjo.com/

(Continued on next page)

Continued

REAGENT or RESOURCE	SOURCE	IDENTIFIER
Other		
SepMate-50	STEMCELL Technologies	85460
Human AB serum heat-inactivated	Valley Biomedical	HP1022HI
Maxpar X8 multi-metal labeling kit	Fluidigm	201300
Antibody stabilizer (PBS-based)	Boca Scientific	131 000
RPMI 1640 media	ThermoFisher	22400-105
Fetal bovine serum	ATCC	30-2020
Bovine serum albumin	Sigma	A3059
Cisplatin	ENZO Life Sciences	ALX-400-040-M250
DNase/RNase-free distilled water	ThermoFisher	10977-023
Cell-ID 20-Plex Pd Barcoding Kit	Fluidigm	201060
Human TruStain FcX for Fc receptor blocking	BioLegend	422302
Cell-I Intercalator-Ir—500 μ M	Fluidigm	201192B
EQ four element calibration beads	Fluidigm	201078
Zombie aqua fixable viability kit	BioLegend	423102

CONTACT FOR REAGENT AND RESOURCE SHARING

Further information and requests for resources and reagents should be directed to and will be fulfilled by the Lead Contact, Alex J. Kuo (alex0229@stanford.edu).

EXPERIMENTAL MODEL AND SUBJECT DETAILS

Human Subjects

Written informed consent was obtained from all participants and the study was conducted in accordance with the guidance of Stanford Research Compliance Office for Human Subject Research. The protocol was approved by Stanford Institutional Review Board (IRB-30494, ACE: Autoimmunity Center of Excellence at Stanford). Bio rep 1 and 2 blood samples from healthy subjects were collected at Stanford Blood Center. All subjects provided a confidential medical history card and completed informed consent to donate blood for clinical or research uses. We exclude subjects with known diseases, including but not limited to HIV, hepatitis and infections, subjects taking medications, or who were pregnant. We specified that the study participants were either < 25 or > 65 in age and CMV-seronegative determined by ELISA. Purification of buffy coat from whole blood was performed at Stanford Blood Center to enrich for leukocytes prior to PBMC isolation. Twin subject inclusion and exclusion criteria and PBMC collection procedures have been described in the influenza vaccination studies reported by [Brodin et al. \(2015\)](#) (PMID: 25594173). We only selected twin subjects who were either between 16 and 21 (younger twins) or between 52 and 72 (older twins) in age, and were CMV-seronegative as determined by ELISA. All samples were from the final blood draw collected 28-days post-vaccination. After sample processing and data collection, a subject from one identical twin pair was found to show signs of upper respiratory tract infection with fever prior to the day 28 visit and was on medications for symptomatic treatment. The twin pair was thus removed from downstream analyses.

METHOD DETAILS

PBMC Isolation

Mononuclear cells were purified from buffy coat by density gradient centrifugation using Ficoll-Paque Plus (GE Healthcare) in SepMate tubes (STEMCELL Technology). Crude PBMCs were treated with RBC lysis buffer (BioLegend) for 5 minutes to remove residual red blood cells followed by 3 PBS washes. Aliquots of 20 million PBMCs were resuspended in human AB serum (Valley Biomedical) containing 5% DMSO (Sigma) for cryopreservation.

Lanthanide Labeling of Antibodies for Mass Cytometry

Antibodies were conjugated with the lanthanides listed in [Tables S1](#) and [S3](#) using MAXPAR antibody labeling kit (Fluidigm), following the manufacturer's protocol. TCEP (ThermoFisher) was added in 100-fold molar excess to generate sulfhydryl groups

for maleimide-mediated conjugation of metal-chelating polymers. Conjugated antibodies were diluted in antibody stabilizing solution (Boca Scientific) containing 0.05% sodium azide (Sigma) for storage.

Mass Cytometry (Sample Processing, Staining, Barcoding and Data Collection)

Cryopreserved PBMCs were thawed and incubated in RPMI 1640 media (ThermoFisher) containing 10% FBS (ATCC) at 37°C for 1 hour prior to processing. Cisplatin (ENZO Life Sciences) was added to 10 μ M final concentration for viability staining for 5 minutes before quenching with CyTOF Buffer (PBS (ThermoFisher) with 1% BSA (Sigma), 2mM EDTA (Fisher), 0.05% sodium azide). Cells were centrifuged at 400 g for 8 minutes and stained with lanthanide-labeled antibodies against immunophenotypic markers in CyTOF buffer containing Fc receptor blocker (BioLegend) for 30 minutes at room temperature (RT). Following extracellular marker staining, cells were washed 3 times with CyTOF buffer and fixed in 1.6% PFA (Electron Microscopy Sciences) at 1×10^6 cells/ml for 15 minutes at RT. Cells were centrifuged at 600 g for 5 minutes post-fixation and permeabilized with 1 mL ice-cold methanol (Fisher Scientific) for 20 minutes at 4°C. 4 mL of CyTOF buffer was added to stop permeabilization followed by 2 PBS washes. Mass-tag sample barcoding was performed following the manufacturer's protocol (Fluidigm). Individual samples were then combined and stained with intracellular antibodies in CyTOF buffer containing Fc receptor blocker (BioLegend) overnight at 4°C. The following day, cells were washed twice in CyTOF buffer and stained with 250 nM 191/193Ir DNA intercalator (Fluidigm) in PBS with 1.6% PFA for 30 minutes at RT. Cells were washed twice with CyTOF buffer and once with double-deionized water (ddH₂O) (ThermoFisher) followed by filtering through 35 μ m strainer to remove aggregates. Cells were resuspended in ddH₂O containing four element calibration beads (Fluidigm) and analyzed on CyTOF2 (Fluidigm) in Stanford Shared FACS Facility. Raw data were concatenated and normalized using calibration beads following the manufacturer's protocol for downstream processing.

Immune Cell Population Definitions (Gating Strategies) and Data Pre-Processing

Raw data were pre-processed using FlowJo (FlowJo, LLC) to identify cell events from individual samples by palladium-based mass tags, and to segregate specific immune cell populations by immunophenotypic markers. A detailed gating hierarchy is described in [Data S2](#). Single-cell data for various immune cell subtypes from individual subjects were exported from FlowJo for downstream computational analyses.

FACS and Western Blotting

Fresh PBMCs or cells recovered from cryopreservation were resuspended in PBS containing Zombie Aqua reagents (Biolegend) and incubated for 15 minutes at RT for viability staining before quenching with CyTOF buffer. Cells were centrifuged at 400 g for 8 minutes and resuspended in CyTOF buffer containing antibodies against immunophenotypic markers for 30 minutes. Markers for sorting: APC anti-CD19 (Biolegend) for B cells, PE-Cy7 anti-CD3 (Biolegend) for T cells, PE anti-CD14 (Biolegend) for monocytes, FITC anti-CD56 (BD) for NK cells, and FITC anti-CD45 (BD) for total PBMCs. Cells were washed once in CyTOF buffer and twice in sorting buffer (PBS containing 0.1% BSA). FACS was performed on sorters in Stanford Shared FACS Facility. Sorted cells collected in CyTOF buffer were centrifuged at 400 g for 8 minutes and resuspended in 5X SDS sample buffer (250mM Tris-HCl pH = 6.8, 10% SDS, 30% glycerol, 5% β -mercaptoethanol, 0.02% bromophenol blue) at 1×10^6 cells per 100 μ l. Samples were sonicated using Bioruptor (Diagenode) for 10 minutes to obtain homogenized lysates for western blot analysis.

Data processing, normalization, and visualization

We normalized single-cell chromatin data to basal levels of histone proteins to account for changes in mark levels due to changes in global amounts of chromatin. We applied a multi-variate linear regression model to each chromatin mark across all cell types and subjects. The model is defined as

$$M_{ij} = \beta_0 + \beta_1 H3_i + \beta_2 H4_i$$

where $H3$ and $H4$ represent the raw values for the respective histone proteins in cell i and M_{ij} is the raw value for a given chromatin mark j in cell i across all cell types and subjects. We defined our normalized chromatin score S_{ij} as the residual of the regression, corresponding to

$$S_{ij} = M_{ij} - \widehat{M}_{ij},$$

where \widehat{M}_{ij} indicates the best fit of the multivariate regression model. We found the residuals were normally distributed, indicating that the linear model adequately fit the data. For each mark after correction, we computed the mean level of the mark in a given cell type across all subjects. We measured heterogeneity between subjects using the inverse of the Simpson's Diversity Index.

Integrated ChIP-seq and transcriptional analysis of lymphoid and myeloid cells (Figures 1E and 1F)

We analyzed genome-wide occupancy of H3K27me3 and H3K4me3 in human CD3⁺ T cells and CD14⁺ monocytes using a published ChIP-seq dataset (GEO: GSE18927) from the Roadmap Epigenomics Mapping Consortium ([Bernstein et al., 2010](#)). We calculated

peak intensity from WIG files as the ratio between read counts for a given peak divided by the length of the peak and by the total sequencing coverage of the sample. Comparisons of peak intensities between different marks and cell types was performed using the Wilcoxon's Rank Sum test. We performed transcriptional analysis of human common lymphoid progenitors and common myeloid progenitors using a published RNA-seq dataset (GEO: GSE74246) (Corces et al., 2016). We identified differentially expressed genes using the DESeq2 algorithm on the read count matrix (Love et al., 2014). We identified genes differentially enriched with chromatin marks between T cells and monocytes, and differentially expressed genes between CLP and CMP using a FDR threshold of 5%. We performed the Gene Ontology (GO) enrichment analysis using the DAVID algorithm (<https://david.ncifcrf.gov>).

Classification of immune cell type using chromatin marks (Figures 2A–2C)

We used the phenotype markers from the standard panels to group cells into five general cell types: T cells, B cells, monocytes, NK cells, and Others. We performed Principal Component Analysis (PCA) to evaluate the ability of chromatin marks to separate immune cell subtypes. Euclidean distances were computed from chromatin modifications profiles between immune cell subsets. We built two L-1 regularized logistic regression models, one for each panel, to distinguish a given cell type from all others using normalized chromatin marks from the bio rep 1 cohort. We validated each of the 10 models in the bio rep 2 cohort using the coefficients obtained from the bio rep 1 cohort. We quantified the accuracy of the models using the area under a receiver operating characteristic curve (AUROC).

Single-cell analysis of the relationship between chromatin mark pairs (Figure 2D)

We quantified the relationship between chromatin mark pairs at a single cell level across all cell types and all subjects using mutual information, which also identifies non-linear relationships. Because of the large number of cells analyzed, a small change in the level of either mark can skew the results. Therefore, for every mark, we excluded all single-cell data points within one standard deviation from the mean. We rescaled the mutual information scores between 0 and 1 by dividing them by their respective channel capacity values (Cover and Thomas, 2012). Finally, we assigned a direction (positive or negative) to our mutual information scores based on the direction of the Spearman's rank correlation for the same pair of chromatin marks. We compared results between bio rep 1 and bio rep 2 by calculating the Pearson's correlation coefficient of the mutual information scores across all mark pairs.

Discovery of chromatin-defined cell subsets in NK cells (Figure 3)

We performed a principal component analysis (PCA) of normalized chromatin marks for NK cells for each individual subject and panel. We tested for the presence of a bimodal distribution along the first principal component using Hartigan's unimodality test. After identifying chromatin-defined NK cell subsets, we estimated their overlap with the known CD56bright/dim NK subsets. We used the mixtools package in R to distinguish CD56bright/dim NK subsets based on CD56 expression using a Gaussian mixture model.

Subject-level analysis of chromatin profiles (Figure 4)

We performed subject level analysis by calculating the mean of the normalized chromatin marks across all cell types and subjects for both panel 1 and panel 2. We combined the means from both panels (separately for standard and T cell focused panels) and integrated multiple batches by applying ComBat normalization (Johnson et al., 2007). We performed ComBat normalization independently for samples profiled using the standard and T cell panels and then combined them afterward. To avoid overlapping measures, we removed data from CD4⁺ and CD8⁺ T cells from the standard panels when combined with the T cell panels. To measure changes in chromatin levels associated with age, we used Hedge's g, defined as a difference of means divided by pooled standard deviation. It has repeatedly been shown to be a robust measure of a difference in means as it accounts for the variance between the two groups being compared (Andres-Terre et al., 2015).

Quantification of cell-to-cell variation in chromatin levels (Figure 5)

We measured cell-to-cell variation in chromatin levels by using the coefficient of variation (CV) (Martinez-Jimenez et al., 2017; Raser and O'Shea, 2004). We computed the CV of single-cell normalized chromatin values for every mark in every cell type for every subject. To avoid negative CV values due to negative means, we systematically added the smallest mean value to all means to solely have positive values. We combined CV values from subjects profiled in the bio rep 1 and bio rep 2 cohorts using ComBat normalization. We used the Wilcoxon's rank sum test to compare CV values between groups, and corrected p values for multiple hypotheses using FDR. We performed transcriptional analysis of using single-cell RNaseq dataset published by Martinez-Jimenez et al. using normalized expression data (Martinez-Jimenez et al., 2017). We computed CV levels for every gene in every subject and calculated difference in mean between old subjects (case) to young (controls). We identified genes bound by H3K27me3 and H3K4m3 using ChIP-seq data published by Wei et al. (2009) on the same cell type profiled by Martinez-Jimenez et al. (CD4⁺ Naive T cells in mouse) and compared them to results obtained using the whole transcriptome using the Wilcoxon's rank sum test.

Heritability analysis of the twin cohort (Figure 6)

We estimated the heritable and non-heritable fraction for each chromatin mark in each cell type using a structural equation model that incorporates additive genetics, common environment, and non-shared Environment (ACE model) (Brodin et al., 2015; Rijdsdijk and Sham, 2002). We implemented the ACE model using the R package OpenMX. We applied the ACE model to measure heritability

across all 800 chromatin mark-cell combinations (40 chromatin marks, 20 cell types). We used ComBat for co-normalizing different batches and different panels. We corrected p values for multiple hypotheses using FDR.

List of R packages

1. sva – ComBat normalization
2. infotheo – mutual information
3. glmnet – L1 penalty LASSO logistic regression
4. diptest – Hartigan's unimodality test for bimodal distribution to identify NK cell subsets
5. mixtools – Identify NK cell subset
6. OpenMX – ACE model for heritability analysis of the twin cohort



levels are shown. The means of chromatin mark and immune cell subset pairs across 12 subjects are used for plotting. Chromatin marks (x axis) and immune cell subsets (y axis) are ordered identically as [Figure 1C](#) for direct comparison. Diameter of circle, subject-to-subject variability measured by Inverse Simpson's Diversity Index.

(B) Validation of EpiTOF data on sorted immune cells. Western blot analysis of the whole-cell extract from sorted immune cells using the indicated antibodies.

(C) Technical reproducibility of EpiTOF platform. Correlation plot of the two technical replicates (6 subjects; 40 chromatin marks; 11 immune cell subsets). Each dot represents the mean of the normalized chromatin mark level in an immune cell subset in a subject. y axis, level in technical replicate 1; x axis, level in technical replicate 2; r, correlation coefficient between the two technical replicates.

(D) Biological reproducibility of EpiTOF analyses. Correlation plot comparing two biological replicates ([Figures 1C](#) and [S1A](#)). Each data point represents the mean of the normalized chromatin mark level in an immune cell subset across 12 subjects. y axis, level in bio rep 1; x axis, level in bio rep 2; r, correlation coefficient between the two biological replicates.

(E) Chromatin modification profiles separate lymphoid and myeloid cells. Dendrogram of unsupervised clustering of immune cell types based on chromatin modification profiles. EpiTOF data from bio rep 2 ([Figure S1A](#)) are shown.

(F) Higher expression of lysine methyltransferases *EZH1* and *EZH2* in T cells than in monocytes. Differential analysis of *EZH1* and *EZH2* expression in T cells over monocytes using publicly available transcription profiling datasets. x axis, effect sizes of differential expression in T cells over monocytes. Error bars, SE.

(G) T cells show higher H3K27me3 but lower H3K4me3 enrichment relative to monocytes. Peak intensity analysis of H3K27me3 (left) and H3K4me3 (right) in T cells (blue) or monocytes (red) using ChIP-seq dataset GEO: GSE18927. p values for the statistical significance of differential enrichment of both chromatin marks are shown.

(H) H3K27me3-enriched genes are largely repressed, whereas H3K4me3-enriched genes are transcriptionally active. Gene expression analysis of H3K27me3-enriched (left) and H3K4me3-enriched (right) genes in T cells (blue) and in monocytes (red). y axis, relative expression in T cells over monocytes. p values for the statistical significance of differential expression are shown.

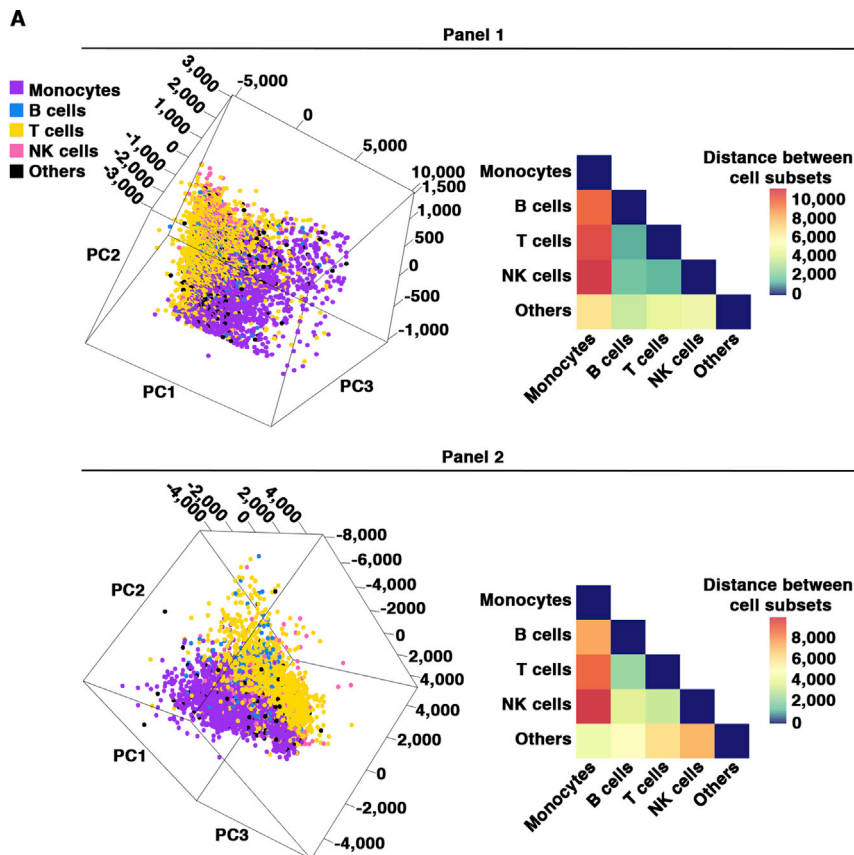


Figure S2. Single-Cell EpiTOF Data Predict Immune Cell Identity and Reveal Covariance between Chromatin Modifications, Related to Figure 2

(A) Separation of immune cells based on variations in chromatin marks. Left, PCA of single-cell dataset from bio rep 2, where each principal component depicts variations in chromatin modification profiles. Analyses using single-cell data collected by EpiTOF panel 1 (top) and 2 (bottom) are shown. Immune cells are color-coded as in Figure 2A. Right, Euclidean distances of chromatin modification profiles between the indicated immune cell subtypes.

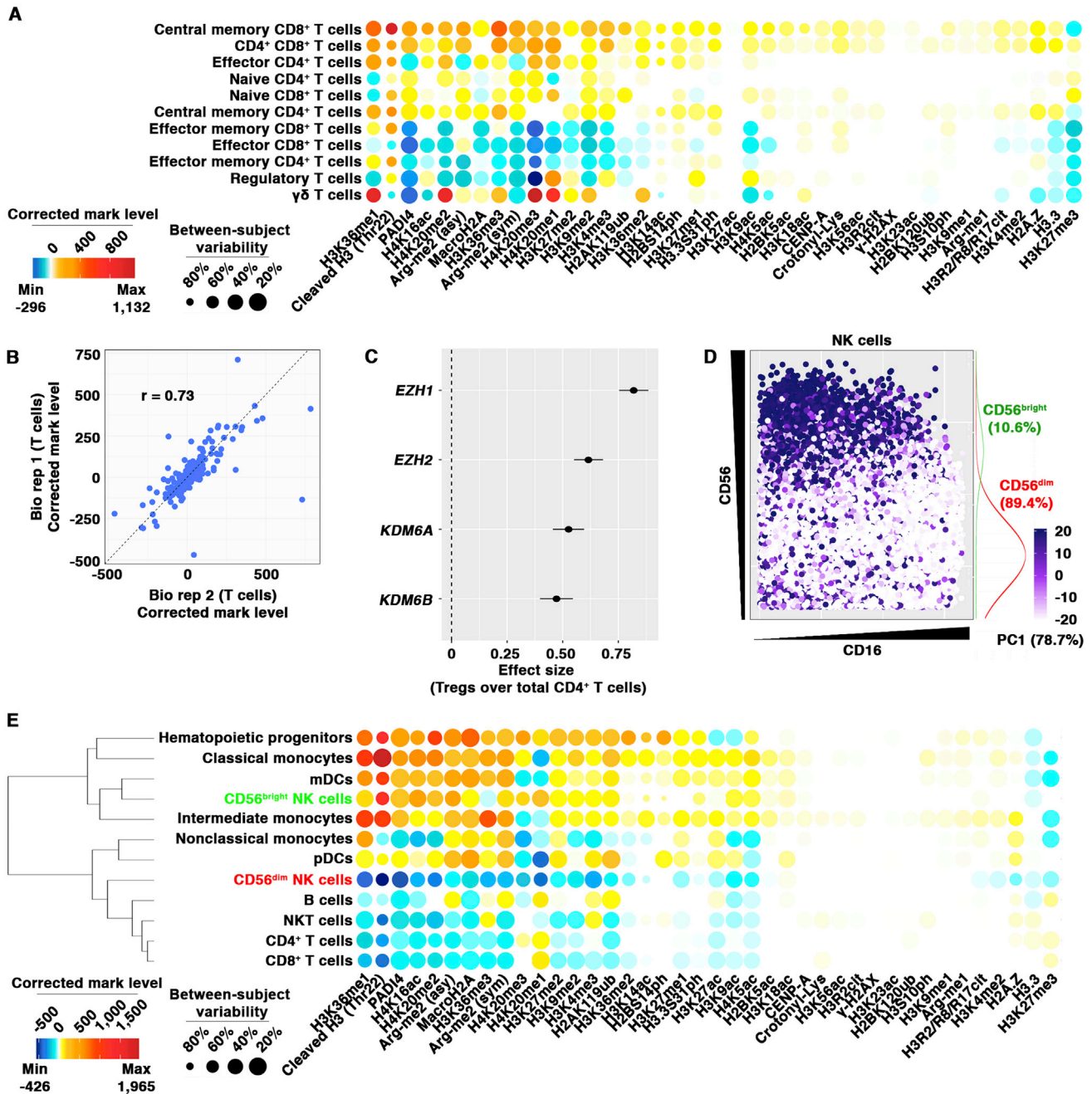


Figure S3. Heterogeneity in Chromatin Modifications in Lymphocytes Originated from Diverse Functional Subsets, Related to Figure 3

(A) Distinct chromatin modification profiles in T cell functional subsets. EpiTOF analysis on bio rep 2 focusing on T cell subgroups. Heatmap representation of the normalized chromatin mark levels as in Figure S1A for the indicated 40 chromatin marks (x axis) in 11 T cell subsets (y axis). The normalized mark levels are centered around the mean of total CD3⁺ T cells. Minimum and maximum values of normalized mark levels are shown. The mean of the level of each chromatin mark and T cell subset pair across 12 subjects is used for plotting. Dendrograms, unsupervised clustering; diameter of circle, subject-to-subject variability measured by Inverse Simpson's Diversity Index.

(B) Biological reproducibility of T cell-focused EpiTOF analysis. Correlation plot comparing EpiTOF data from the two biological replicates. Each data point represents the mean of the level of a chromatin modification in a T cell subtypes. y axis, level in bio rep 1; x axis, level in bio rep 2; r, correlation coefficient between the two biological replicates.

(C) The expression of lysine methyltransferases and demethylases regulating H3K27 methylation is elevated in regulatory T cells. Forest plot showing the effect sizes of the expression of the indicated genes in Treg over total CD4⁺ T cells. Error bars, SE.

(D and E) Variations of chromatin modification profiles segregate NK cells into two subsets. Scatterplot of NK cells from bio rep 2 plotted based on CD56 (y axis) and CD16 (x axis) levels. Color, principal component 1 summarizing the variance of 20 chromatin marks measured by EpiTOF panel 1. Density plot

(legend continued on next page)

depicts the frequencies of the indicated subpopulations segregated by MixTool ([Benaglia et al., 2009](#)) using CD56 level. Green, CD56^{bright}, red, CD56^{dim} (D). Heatmap analysis of both NK cell subsets with other immune cell populations. Chromatin marks at x axis are ordered identically as [Figure 1C](#) for direct comparison. Dendrogram at y axis, unsupervised clustering; diameter of circle, subject-to-subject variability measured by Inverse Simpson's Diversity Index (E).

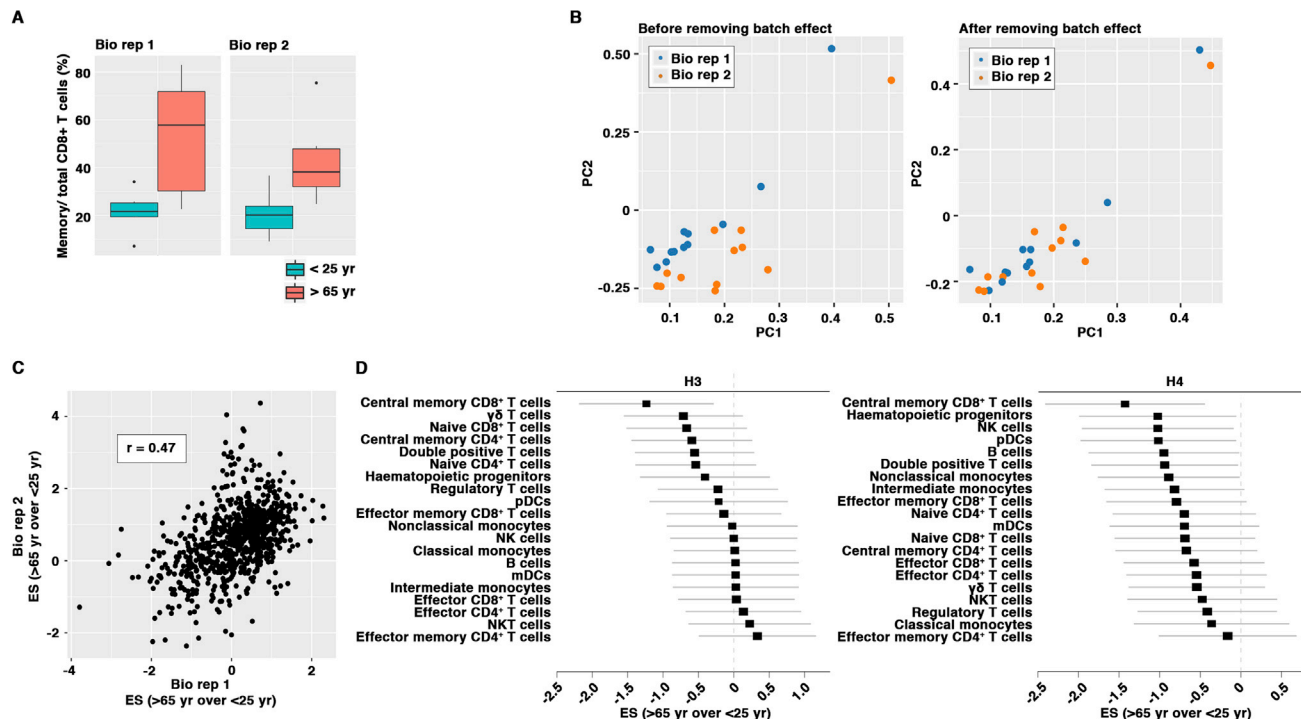


Figure S4. Increased Variations in Chromatin Modification Profiles with Aging, Related to Figure 4

(A) Elevated proportion of memory CD8⁺ T cells in older subjects. Boxplots showing the percentage of memory subsets in CD8⁺ T cells in the subjects from the indicated age groups in bio rep 1 (left) or 2 (right). Salmon, > 65 years; cyan, < 25 years.

(B) Integration of the two biological replicates for aging-related analyses. PCA of EpiTOF datasets before (left) and after (right) batch effect removal by empirical Bayes framework. Each dot represents a subject from bio rep 1 (blue) or 2 (orange). Principal components are computed based on the variation of 40 chromatin marks in 20 immune cell subsets (800 data points).

(C) Biological reproducibility of the altered chromatin modification profiles with aging. Correlation plot of the effect sizes comparing the levels of each chromatin mark and cell type pairs between age groups (older over younger). Each dot represents the effect size calculated from the two biological replicates. x axis, effect size from bio rep 1; y axis, effect size from bio rep 2; r, correlation coefficient between biological replicates.

(D) Histone loss in central memory CD8⁺ T cells with age. Forest plots depict meta-analyses of effect sizes of total histone H3 (left) and H4 (right) levels in the indicated cell subsets from the two biological replicates. Effect sizes, histone levels in older over younger subjects. Error bars, SE.

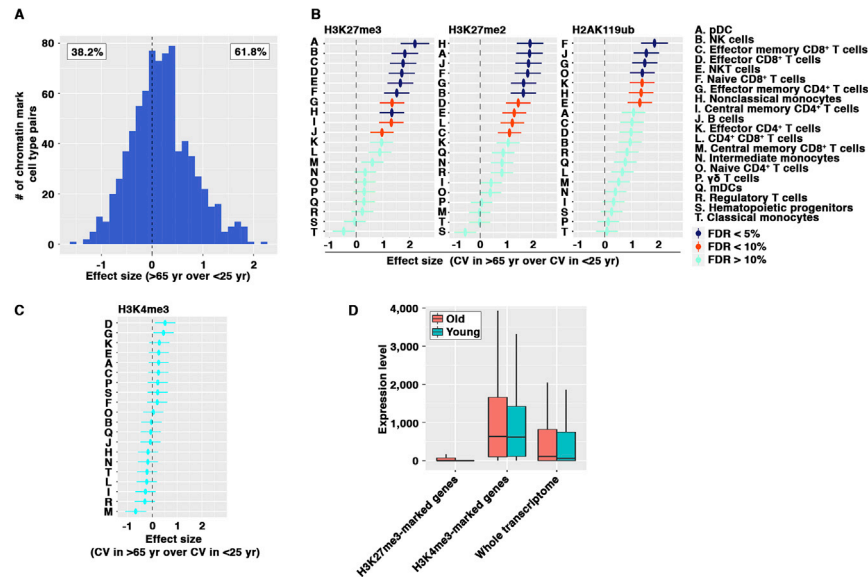


Figure S5. Increased Single-Cell Variability in Chromatin Modification Profiles with Age, Related to Figure 5

(A) Single-cell variability of chromatin modifications is higher in older subjects. Histogram showing the number of chromatin mark and cell type pairs (y axis) with effect sizes (x axis) comparing cell-to-cell variability (CVs) between the two age groups at the indicated levels. Effect size, CV in older subjects over CV in younger subjects. Dashed line, effect size = 0.

(B) PRC-mediated modifications show higher single-cell variations with aging across several immune cell subsets. Forest plots depict the effect sizes of CVs of H3K27me3 (left), H3K27me2 (middle), and H2AK119ub (right) between age groups in the indicated immune cell subsets. Effect size (x axis), CV in older subject over CVs in young subjects. Immune cell subsets (y axis) are ranked by FDR. Dark blue, FDR < 5%; red, FDR < 10%; light blue, FDR > 10%. Error bars, SE.

(C) Single-cell variability of H3K4me3 is not altered significantly with age. Forest plot shows the effect sizes of CVs of H3K4me3 between age groups in the indicated immune cell subsets. Effect size (x axis), CV in older subject over CVs in young subjects. Immune cell subsets (y axis) are ranked by FDR. All tests have FDR > 10%. Error bars, SE.

(D) H3K27me3 marks transcriptionally repressed genes while H3K4me3-marked genes are actively transcribed. Expression levels of the indicated subsets of genes in naive CD4⁺ T cells purified from old (salmon) or young (cyan) *M. musculus domesticus*. Transcription profiling data and lists of genes occupied by H3K27me3 or H3K4me3 are derived from publicly available scRNA-seq (Martinez-Jimenez et al., 2017) and ChIP-seq (Wei et al., 2009) datasets, respectively. Transcriptome-wide gene expression levels are shown.

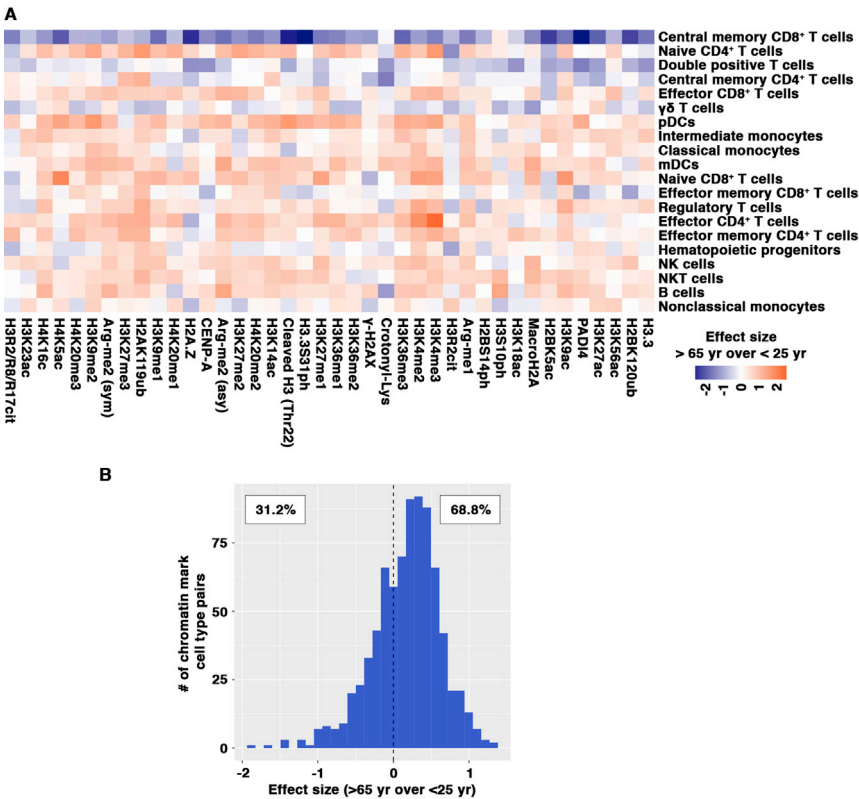


Figure S6. Increased Variations of Chromatin Modifications with Aging Are Largely Driven by Non-heritable Influences, Related to Figure 6

(A) Altered chromatin modification profiles with aging. Heatmap representation of the effect sizes of the levels of the indicated chromatin mark and cell type pairs comparing between twin subjects from the two age groups. The marks and cell subsets are ordered as the heatmap in Figure 4C for direct comparison. Effect size, chromatin mark levels in older twin subjects over the levels in younger twin subjects.

(B) Single-cell variability of chromatin modifications is higher in older twin subjects. Histogram showing the number of chromatin mark and cell type pairs (y axis) with the indicated level of effect sizes comparing single-cell CVs between twin subjects from the two age groups. Effect size, CV in older twin subject over CV in young twin subject. Dashed line, effect size = 0.